ASTROCYTE-SECRETED FACTORS IN FRAGILE X MICE

EXPRESSION PATTERNS OF HEVIN AND SPARC IN THE FRAGILE X MOUSE— IMPLICATIONS FOR THALAMOCORTICAL SYNAPSE DEFICITS

By

JESSICA WALLINGFORD

A Thesis Submitted to the School of Graduate Studies

In Partial Fulfillment of the Requirements

For the Degree

Master of Science

McMaster University

MASTER OF SCIENCE (2016) McMaster University
(Science—Neuroscience, MiNDS) Hamilton, Ontario

TITLE: Expression Patterns of Hevin and SPARC in the Fragile X Mouse—Implications for Thalamocortical Synapse Deficits

AUTHOR: Jessica Wallingford

SUPERVISOR: Dr. Laurie C. Doering

NUMBER OF PAGES: xii, 83

ABSTRACT

Astrocytes are required for the proper development of synapses within the brain and astrocyte dysfunction has been indicated in many neurodevelopmental disorders, including Fragile X Syndrome (FXS). FXS is characterized by a deficiency in fragile X mental retardation protein (FMRP). FMRP regulates the translation of numerous mRNAs and its loss disturbs the composition of proteins for dendritic spine and synapse development. Here we investigate whether particular astrocyte-derived factors that have been implicated in governing excitatory synapse development in the brain show altered expression within the context of FXS. Using *Fmr1* knock-out (KO) mice lacking FMRP, we analyzed the early postnatal protein expression of the astrocyte-secreted factors hevin, SPARC, and glypicans 4/6 in the cortex and hippocampus (regions in which dendritic spine abnormalities have been associated with FXS) via Western blotting. Hevin and SPARC showed altered expression patterns in *Fmr1* KO mice, compared to WT, in a brain-region-specific manner. In the cortex, we found a transient increase in the level of hevin in P14 *Fmr1* KO mice, compared to WT, as well as decreases in *Fmr1* KO levels of SPARC at P7 and P14. In the hippocampus, hevin expression was lower in P7 *Fmr1* KO mice than in WT mice, and then surpassed WT levels by P21. Hevin is involved in the proper establishment of thalamocortical synapses, and so, we also examined the number of thalamocortical synapses formed in co-cultures of WT thalamic and cortical neurons with either WT or KO astrocytes. Preliminary data from these experiments show an increase in the number of thalamocortical synapses formed when WT neurons were cultured with KO astrocytes, suggesting the involvement of astrocytes in the proper development of thalamocortical connectivity. Together, these findings indicate aberrant astrocyte-signalling in FXS and suggest that altered expression of hevin and SPARC may contribute to abnormal neurobiology in FXS.

ACKNOWLEDGEMENTS

This thesis represents the culmination of a two-year process of research and experimentation, and as all scientists will know, such a process is both difficult and uncertain. For in addition to the many hours of research required for any project that seeks to uncover some further knowledge, research undertaken through the laboratory setting includes the constant risk of malfunction, mistiming, and the recalcitrance of nature. Against these obstacles, one cannot succeed without a network of support.

At the fore of this network stands my supervisor, Dr. Laurie C. Doering. Without the manifold resources made available by his laboratory, without his willingness to allow me the freedom to pursue leads and hints, and without his constant and supportive presence, this research would not have achieved its current state. To Dr. Doering I extend my deepest professional gratitude.

I could not, moreover, fail to acknowledge the guidance I received from my lab mates, Connie Cheng, Angela Scott, Mary Sourial, Shivraj Jhala, and Amanda Poxon—I would especially like to thank Amanda for all of the hours that she spent helping me towards the end of my experiments. To work in close proximity amongst such dedicated scientists and researchers has been invigorating. For the collaborative environment of the laboratory and for the support – both academic and personal – of these talented individuals, I am grateful.

To the members of my committee, Dr. Jane Foster and Dr. Ram Mishra, I extend my appreciation. This project has benefited from their feedback, criticism, and guidance. An external perspective is a requisite to good research.

I would also like to thank the members of the Ball and West-Mays Labs, Tom Sabljic, Paula Deschamps, Vanessa Martino, Monica Akula, Anna Korol, Scott Bowman, Emily Anne

Hicks, and Dr. Aftab Taiyab. It was a joy to benefit from the resources and knowledge of this capable community, of which I am grateful to have been a part.

Lastly, I must extend my love and gratitude to my family.

My mother and father, Pierce and Courtney, have never ceased to support me in these many years of post-secondary education. The expense, the stress, the uncertainty of the results have not deterred them in their acceptance of this chosen field. For this, I count myself truly lucky.

From my partner and his family, I have benefitted from much support and, what is more, from a broad perspective on the nature of this endeavor. Their appreciation of the value of knowledge is not to be unrecognized.

Will—many thanks for many conversations.

TABLE OF CONTENTS

LIST OF FIGURES

LIST OF TABLES

LIST OF ABBREVIATIONS

AMPA, α-amino-3-hydroxy-5-methyl-4-isoxazole propionic acid

ASD, autism spectrum disorders

DIV, days *in vitro*

Fmr1, fragile X mental retardation 1

FMRP, fragile X mental retardation protein

FXS, Fragile X syndrome

GFAP, glial fibrillary acidic protein

GluA1, glutamate receptor subunit 1

GPC 4/6, glypican 4 and 6

HRP, horse radish peroxidase

KO, knock-out

LTD, long-term depression

MAP2, microtubule associated protein 2

MACS, magnetic-activated cell sorting

mGluR, metabotropic glutamate receptor

NMDA, N-methyl-D-aspartate

NL1B, Neuroligin-1B

NMM, Neural maintenance media

Nrx1α, Neurexin-1α

P, postnatal day

PBS, phosphate-buffered saline

PSD95, post-synaptic density protein 95

RGC, retinal ganglion cell

SEM, standard error of the mean

SMECs, spines with multiple excitatory contacts

TBS-T, tris-buffered saline solution with Tween-20

TSP, thrombospondin

VGlut1, vesicular glutamate transporter 1

VGlut2, vesicular glutamate transporter 2

WT, wild-type

CHAPTER ONE

GENERAL INTRODUCTION

1.1 Fragile X Syndrome

Fragile X syndrome (FXS), the most common inherited single-gene cause of autism spectrum disorders (ASD) and cognitive impairment (reviewed in Lubs et al., 2012; Wang et al., 2012), is a neurodevelopmental disorder affecting approximately 1 in 5000 males and about half as many females (Kaufmann et al., 2004; Coffee et al., 2009). Individuals with FXS can exhibit mild to severe cognitive impairment, autistic behaviors, attention deficits, hyperactivity, susceptibility to seizures, hypersensitivity to sensory stimuli, disrupted sleep, macroorchidism, and craniofacial abnormalities, as well as an assortment of neurobiological abnormalities (Comery et al., 1997; Beckel-Mitchener and Greenough, 2004; Nimchinsky et al., 2001; Kronk et al., 2010). As a monogenic neurodevelopmental disorder, FXS has been an invaluable model for a broader understanding of ASDs, for which the etiology is vastly heterogeneous.

FXS (initially termed Martin-Bell Syndrome) was first documented in 1943 when Martin and Bell described a family in which 11 males born over two generations to mothers of 'normal intelligence' showed severe cognitive impairment (Martin and Bell, 1943). Martin and Bell noted the stationary mental state of afflicted individuals, suggesting that this condition was a defect of development. In 1969, Lubs studied a family demonstrating cognitive impairment in keeping with a pattern of X-linked inheritance and identified a constriction site (or 'fragile site') near the end of the long arm of the X chromosome. This constriction site on the X chromosome was later demonstrated in the Martin-Bell pedigree described above (Richards et al., 1981). Verkerk et al., (1991) mapped the Fragile X mental retardation 1 (FMR1) gene to this fragile-X locus.

FXS is predominantly caused by a repeat expansion of a CGG trinucleotide in the 5' non-coding region of the *FMR1* gene located at Xq27.3 (Harrison et al.,1983; Fu et al., 1991). Under normal conditions, this region contains between 5 and 45 CGG repeats. Alleles containing

numbers of CGG repeats that fall within the ranges of 45- 55 or 55-200 are classified as grey-zone and premutation alleles, respectively, and have the tendency to expand in subsequent generations (Fernandez-Carvajal et al., 2009; Yrigollen et al., 2014). An expansion of greater than 200 CGG repeats constitutes the full FXS mutation (Oberlé et al., 1991). This leads to the hypermethylation and consequent silencing of the *FMR1* gene, resulting in the loss of its protein product, fragile X mental retardation protein (FMRP; 70-80 kDa) (Pieretti et al., 1991; Hou et al, 2006; Garber et al., 2008; Santoro et al., 2012).

1.2 The *Fmr1* KO mouse model of Fragile X Syndrome

The *Fmr1* mouse gene shows 97% homology to the human gene (Ashley et al., 1993), making the mouse an excellent candidate to model FXS. In 1994, a Fragile X transgenic mouse model (FVB.129p2(B6)-*Fmr1*) was developed by Bakker et al., in which the *Fmr1* gene is knocked-out such that no functional FMRP is produced. This allowed for a more detailed examination of the molecular and cellular mechanisms underpinning FXS neurobiology. This mouse model re-capitulates many of the features observed in humans including learning deficits (Bakker et al., 1994), attention deficits (Nielson et al., 2002), hyperactivity (Oostra and Hoogeveen, 1997; Qin et al., 2002), susceptibility to seizures (Bakker et al., 1994; Chen and Toth, 2001), macroorchidism (Bakker et al., 1994), and neurobiological abnormalities (Pfeiffer and Huber, 2009).

The development and use of animal models to study FXS has led to sizeable advancements in our understanding of the altered cellular and molecular mechanisms that give rise to the various synaptic pathologies defining FXS. This knowledge has, in turn, led to the development of several strategies for targeted pharmacological treatments of FXS (reviewed in

Berry-Kravis, 2014 and Wang et al., 2015). However, many challenges have ensued for the effective translation and application of findings from animal studies to human trials—Much work remains to better understand and effectively treat this highly complex neurodevelopmental disorder.

1.3 FMRP

The protein product of the *FMR1* gene, FMRP, is expressed ubiquitously, with relatively higher expression in the central nervous system (Santoro et al., 2012; Sidorov et al., 2013). Within the brain, FMRP expression is highest in the hippocampus, cortex, and cerebellum (Bakker et al., 2000) and has been identified in neurons (Sidorov et al., 2013), as well as in oligodendrocyte precursor cells (Wang et al., 2004) and the astrocyte cell lineage (Pacey and Doering, 2007). FMRP influences synaptic development through its ability to bind, transport, and regulate the local translation of several mRNAs corresponding to synaptic proteins (reviewed in Bhakar et al., 2012). An estimated four percent of total brain mRNA binds FMRP (Darnell et al., 2011), and its absence in FXS has been associated with altered synapse structure, number, and function (reviewed in Pfeiffer and Huber, 2009). As such, FMRP deficiency and the consequent aberrant protein synthesis and expression is thought to underlie FXS synaptopathy (Kelleher & Bear, 2008; Darnell et al., 2011). Importantly, the various abnormal synapse phenotypes that have been reported in the literature seem to be highly dependent upon the stage of development and the brain region studied.

A well-studied example of an FMRP-related synaptopathy involves the group 1 metabotropic glutamate receptors (mGluRs; mGluR1s and mGluR5s) in the hippocampus. Under normal conditions, the activation of group 1 mGluRs leads to the local synthesis of FMRP,

which can then negatively regulate its mRNA targets, many of which encode long-term depression (LTD) proteins (reviewed in Krueger & Bear, 2011). In FXS, a lack of FMRP results in excessive protein synthesis and exaggerated LTD in response to group 1 mGluR activation (Huber et al. 2002; Bear et al., 2004). Alternatively, there is accumulating evidence demonstrating hyperexcitability of cortical circuits, illustrating the region-specificity of abnormal synapse phenotypes in FXS (reviewed in Contractor et al., 2015). Additionally, numerous studies examining the altered neurobiology associated with the absence of FMRP have focused on changes at the level of dendritic spines, the primary site for excitatory connections between neurons (Ianov et al., 2009). Studies of FXS in humans or animal models have described a significant increase in the number of dendritic spines associated with FXS, with a greater proportion of immature spine phenotypes (i.e. long, thin, tortuous dendritic spines) (Comery et al., 1997; Irwin et al., 2001; Nimchinsky et al., 2001).

1.4 Astrocytes and the synapse

Recently, astrocytes have emerged in the literature as important regulators of synapse development and have been shown to promote both synapse formation and maturation (reviewed in Allen et al., 2013; Chung et al., 2015). It is estimated that the processes from a single astrocyte can make contact with up to 10^5 synapses (Bushong et al., 2002; Halassa et al., 2007). *In vitro* research has demonstrated that retinal ganglion cells (RGCs) cultured with an astrocyte feeder layer formed seven-fold more functional excitatory synapses than RGCs cultured alone (Ullian et al., 2001), illustrating the importance of astrocytes to developing neural networks. The mechanisms by which astrocytes regulate neural connectivity in the brain have not been studied in depth. However, in recent years, several astrocyte-secreted factors have been implicated in the

astrocyte-mediated mechanisms of synapse development (reviewed in Corty and Freeman, 2013). Several of these identified astrocyte-secreted factors include cholesterol (Mauch et al., 2001), tenascin-C (Barros et al., 1992; Bartsch et al., 1992; Faissner et al., 2010), thrombospondins (TSPs) 1 and 2 (Christopherson et al., 2005), hevin (Kucukdereli et al., 2011), SPARC (Jones et al., 2011; Kucukdereli et al., 2011), and glypicans 4 and 6 (Allen et al., 2012), of which the latter three will be discussed in greater detail below. Further research is required to better understand the astrocyte-neuron interactions that govern the development of neural networks.

1.5 Astrocytes and Fragile X Syndrome

The expression of FMRP was previously thought to be exclusive to neurons (Feng et al., 1997), and so, research examining the consequences of a deficiency in FMRP has largely focused on FMRP (or a lack there of) in neurons. However, research from our lab has shown that FMRP is also expressed in astrocytes during development (Pacey and Doering, 2007). Just as a lack of FMRP in neurons leads to aberrant protein synthesis in neurons, a lack of FMRP may disturb the protein milieu in astrocytes and lead to dysregulated astrocyte-neuron interactions. Using an *Fmr1* KO mouse model of FXS, research from our lab has shown abnormal dendrite morphology and altered synaptic protein expression in wild-type (WT) hippocampal neurons co-cultured with *Fmr1* KO astrocytes (Jacobs and Doering 2010). Moreover, dendritic and synaptic abnormalities were prevented when *Fmr1* KO hippocampal neurons were co-cultured with WT astrocytes. Furthermore, recent work in our lab indicates that astrocyte-conditioned media can also prevent abnormal dendrite and synapse abnormalities, carrying implications for the role of soluble factors secreted from astrocytes in FXS (unpublished data). Additionally, recent research

using an astrocyte-specific conditional *Fmr1* KO mouse model has demonstrated that an *in vivo* lack of FMRP specifically in astrocytes contributes to synaptic deficits in the cortex (Higashimori et al., 2016).

1.6 Astrocyte-secreted factors hevin, SPARC, and glypicans 4 and 6

As discussed above, astrocyte-secreted factors can play regulatory roles, both positive and negative, in the development, maturation, and maintenance of synapses (Fig. 1). This thesis focuses on the early postnatal expression patterns of the astrocyte-secreted factors, hevin, SPARC, and glypicans 4 and 6, which will each be discussed in greater detail below.

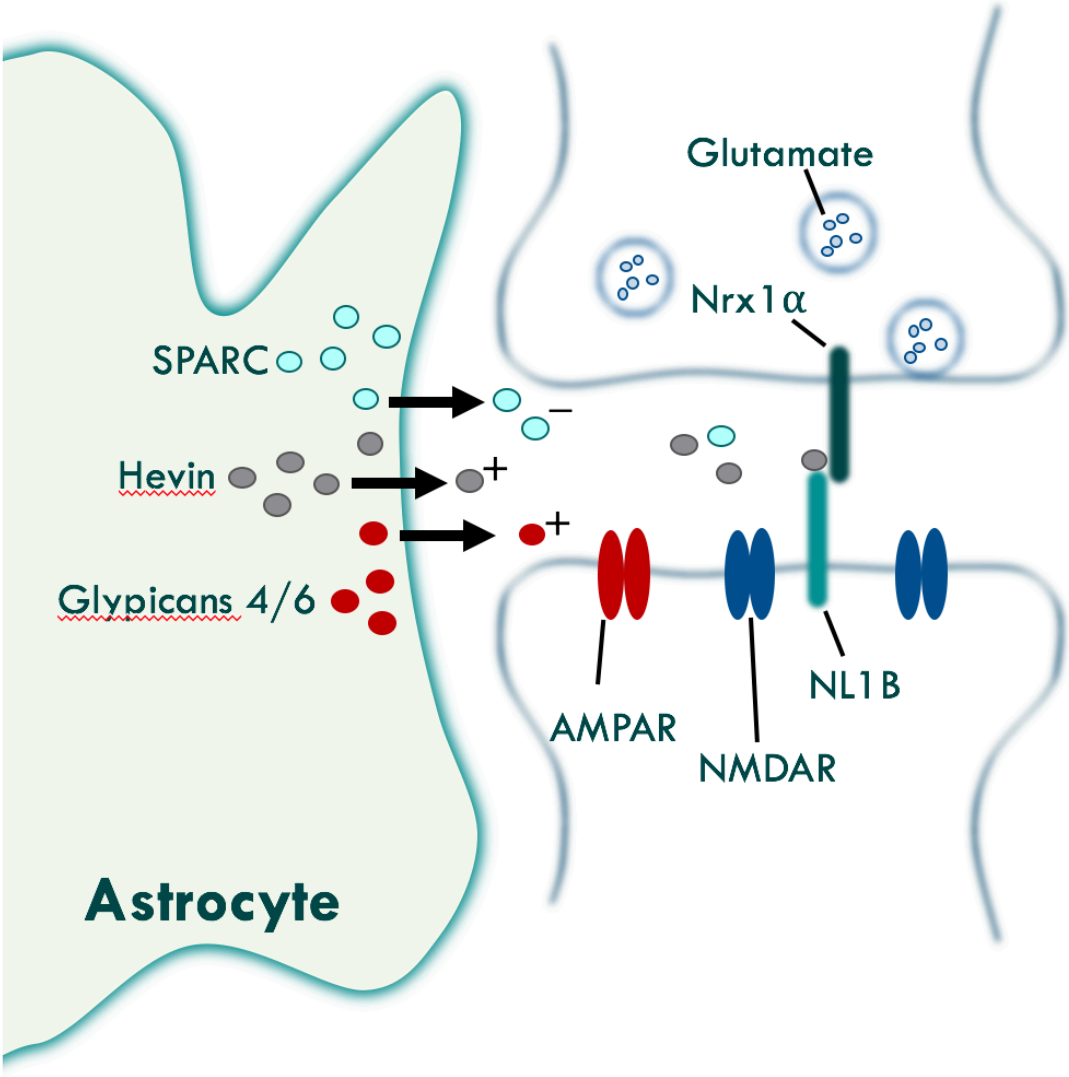
Glutamate
Nrx1α
SPARC
Hevin
Glypicans 4/6
AMPAR
NMDAR
NL1B
Astrocyte

Figure 1. Astrocytes secrete positive and negative regulators of excitatory synapse development. Abbreviations: AMPAR, α-amino-3-hydroxy-5-methyl-4-isoxazole propionic acid receptor; NMDAR, N-methyl-D-aspartate receptor; NL1B, neuroligin-1B; Nrx1α, neurexin-1α.

1.5.1 Hevin

The matricellular protein hevin (~130 kDa; also known as synaptic cleft-1 or SPARC-like 1) is highly expressed in astrocytes during development and this expression is maintained in the adult (Mendis & Brown, 1994; Cahoy et al., 2008; Eroglu, 2009). Western blots from both the superior colliculus and whole cortical tissue homogenates show that hevin expression peaks at approximately P14-P25, roughly coinciding with peak synaptogenic activity (Kucukdereli et al., 2011; Risher et al., 2014). Darnell et al. (2011) has identified hevin as a specific mRNA target of FMRP. Hevin is capable of inducing excitatory synapse formation *in vitro*, as evidenced by a three-to fivefold increase in the number of synapses per cell observed in RGCs cultured with hevin, compared to RGCs cultured alone (Kucukdereli et al., 2011). Moreover, *Hevin* KO mice show a decrease in the number of RGC-collicular synapses, providing evidence of an *in vivo* role for hevin in synapse formation. More recently, hevin has been shown to function as a trans-synaptic linker between presynaptic neurexin-1α and post-synaptic neuroligin-1B (Singh et al., 2016; Fig. 2). In this way, hevin assists in the formation of synapses expressing this particular neurexin and neuroligin pair, a category that includes both thalamocortical synapses and RGC-collicular synapses. Of note, while hevin induces the formation of synapses that appear ultrastructurally normal, whole-cell patch clamp recordings demonstrate that these synapses are post-synaptically silent (Kucukdereli et al., 2011). The inability of these 'silent' synapses to facilitate neurotransmission can be attributed to a lack of postsynaptic α-amino-3-hydroxy-5-methyl-4-isoxazole propionic acid receptors (AMPARs). This suggests the presence of additional astrocyte-secreted factors that regulate post-synaptic function.

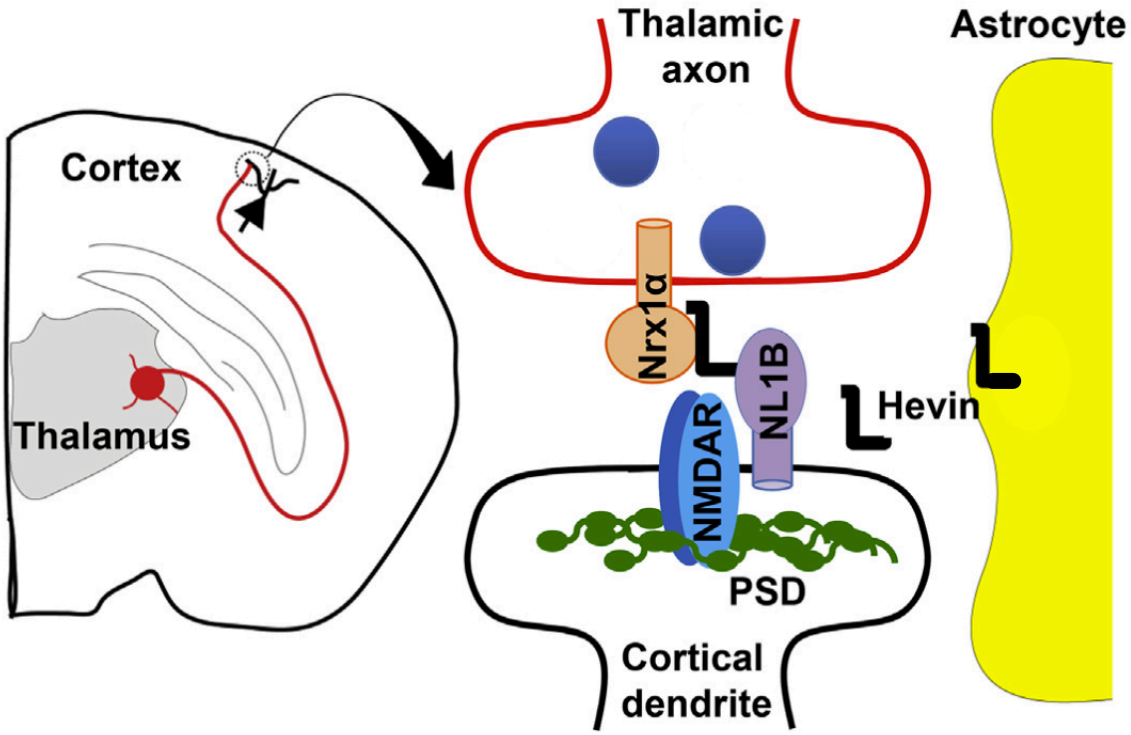
Thalamic
axon
Astrocyte
Cortex
Nrx1α
NL1B
Hevin
Thalamus
NMDAR
PSD
Cortical
dendrite

Figure 2. Hevin establishes excitatory thalamocortical synapses by bridging presynaptic neuroligin-1B and postsynaptic neurexin-1α. Abbreviations: NL1B, neuroligin-1B; Nrx1α, neurexin-1α**.** Modified from Singh et al., 2011.

1.5.2 SPARC

While purified hevin was capable of inducing excitatory synapse formation in RGC cultures, ACM depleted of TSPs (a family of well-characterized astrocyte-secreted synaptogenic proteins (Christopherson et al., 2005)), but still containing hevin, showed no synaptogenic activity (Kucukdereli et al., 2011). This finding suggested the presence of an ACM component capable of inhibiting the synaptogenic function of hevin. The hevin homologue, SPARC, was identified as this inhibitory factor (Kucukdereli et al., 2011).

SPARC is highly expressed by astrocytes in the developing brain (although not as highly as hevin) and is also expressed in the adult brain (Eroglu, 2009). SPARC does not interfere with TSP function and thus the inhibitory activity of SPARC is specific to the synaptogenic function of hevin (Kucukdereli et al., 2011), although the mechanism by which SPARC interferes with hevin remains unknown. While hevin KO mice show a decrease in RGC-collicular synapses, *SPARC* KO mice show an increase, providing *in vivo* support for the proposed antagonistic relationship between these two factors. Due to the nature of the relationship between hevin and SPARC, it is important to consider the expression patterns of both of these factors together, rather than the expression pattern of each individually.

1.5.3 Glypicans 4 and 6

In addition to hevin and SPARC, astrocytes also express the heparan sulfate proteoglycans glypican 4 and its closest homolog glypican 6 (De Cat and David, 2001), which regulate excitatory synapse formation and post-synaptic function (Allen et al., 2012). During development, glypican 4 and 6 mRNA is expressed throughout the brain and is enriched in astrocytes compared to neurons (Cahoy et al., 2008; Allen et al., 2012). Glypican 4 mRNA shows highest expression in the hippocampus, while glypican 6 mRNA is enriched in the

cerebellum. Allen et al. (2012) identified glypicans 4 and 6 as astrocyte-conditioned media components, capable of inducing functional glutamatergic synapse formation in RGC cultures. This study subsequently established that glypicans 4 and 6 are involved in the recruitment of glutamate receptor subunit 1 (GluA1) containing AMPA receptors to the postsynaptic membrane, thus inciting post-synaptic function. Additionally, *Glypican 4* KO mice exhibit reduced mEPSC amplitudes in measurements from hippocampal slices as well as reduced surface levels of GluA1.

CHAPTER TWO

RATIONALE, CENTRAL HYPOTHESIS, AND RESEARCH AIMS

2.1 Rationale for the study

Abnormal astrocyte function has been linked to many neurodevelopmental disorders, including FXS (reviewed in Sloan and Barres, 2014), however, the role of astrocytes in FXS is not yet well understood. Recently, several astrocyte-secreted factors that regulate the development of various synaptic populations have been identified (reviewed in Corty and Freeman, 2013). Given the role of astroycte-secreted factors in governing synapse development and the wide range of abnormal synaptic phenotypes presented in FXS (reviewed in Pfeiffer and Huber, 2009), it is probable that particular astrocyte-secreted factors are involved in mechanisms underlying synaptic pathologies in FXS. Importantly, our findings support the notion that astrocyte-signaling is dysregulated in FXS and stress the significance of astrocyte-mediated mechanisms in the neurobiological deficits that characterize FXS.

2.2 Central hypothesis

Altered levels of the astrocyte-secreted factors hevin, SPARC, and/or glypicans 4 and 6 during development contribute to neurobiological deficits in FXS.

2.3 Research Aims

2.3.1 Determine in vivo early postnatal expression levels of the astrocyte-secreted factors hevin, SPARC, and glypicans 4 and 6.

Hevin, SPARC, and glypican 4 and 6 have each been implicated in the regulation of synapse development (Kucukdereli et al., 2011; Allen et al., 2012). Therefore, we compared the expression of hevin, SPARC, and glypican 4 and 6 in the developing cortex and hippocampus,

both of which have high levels of FMRP (Bakker et al., 2000), of wild-type (WT) mice and mice that do not express FMRP (*Fragile X mental retardation 1* [*Fmr1*] KO). Samples were collected from pups aged P7, P14, and P21 and were analyzed via Western blotting for their respective protein contents.

2.3.2 Assess the number of thalamocortical excitatory synapses formed in astrocyte-neuron co-cultures.

Hevin directly assists in the establishment of thalamocortical excitatory synapses, but not corticocortical excitatory synapses (Risher et al., 2014; Singh et al., 2016). Therefore, we sought to determine whether there were differences in the number of thalamocortical excitatory synapses in co-cultures consisting of thalamic neurons, cortical neurons, and either WT astrocytes or *Fmr1* KO astrocytes. Thalamocortical synapses were identified by the co-localization of $VGlut2^{+}$ and $PSD95^{+}$ puncta.

CHAPTER THREE

EXPERIMENTAL DESIGN

3.1 Animals

WT and *Fmr1* KO mice (FVB.129P2[B6]-*Fmr1*^{tm1Cgr}) were housed and bred in the McMaster University Central Animal Facility. All experiments and animal-handling procedures followed the guidelines set by the Canadian Council on Animal Care and were approved by the McMaster Animal Research Ethics Board.

3.2 Brain Tissue Collection

WT and *Fmr1* KO male pups at the age of P7, P14, and P21 were decapitated and whole brains were extracted. Extracted brains were immediately placed into ice-cold, sterile 0.01 M phosphate-buffered saline and cortical and hippocampal tissue was isolated from each brain. Samples were immediately placed into separate microcentrifuge tubes, snap-frozen on dry ice, and subsequently stored at -80°C. Each sample of cortical or hippocampal tissue consisted of tissue from a single hemisphere. In addition, the tails from 8 randomly selected pups (4 pups from each genotype, WT and *Fmr1* KO) were collected and the genotypes of the mice were confirmed for each group.

Samples intended for hevin analysis were mechanically homogenized on ice in lysis buffer (0.05 M Tris [pH 7.5], 0.5% Tween-20, 10mM EDTA, Roche ULTRA protease inhibitor tablet, Roche PhosSTOP phosphatase inhibitor tablet). Homogenates were left on ice for 15 min and then centrifuged at 2350 x g for 10 minutes at 4°C. Samples intended for SPARC and glypican 4 and 6 analysis were mechanically homogenized on ice in RIPA buffer (150 mM NaCl, 1% NP40, 0.5% Deoxycholic Acid, 0.1% SDS, 50 mM Tris [pH 8.0], Roche ULTRA protease inhibitor tablet, Roche PhosSTOP phosphatase inhibitor tablet). Homogenates were left on ice for 1 hour and then centrifuged at 16000 x g for 15 min at 4°C. The protein concentration

of all supernatants were determined by a DC protein assay (Bio-Rad, Mississauga, ON, CA). Samples were aliquoted and stored at -80°C.

3.3 Western Blotting

Cortical and hippocampal samples containing either 30µg (for hevin and SPARC Westerns) or 50µg (for glypican 4 and 6 Westerns) of protein were combined with 2X Laemmli Sample Buffer (Bio-Rad). Samples were heated for 5 minutes at 95°C, centrifuged briefly, and immediately loaded onto a gradient 4-15% precast polyacrylamide stain-free gel (Bio-Rad) for electrophoresis. Each gel contained age-matched WT and *Fmr1* KO samples (n=4/group) isolated from either the cortex or hippocampus. Two gels were run for each time-point and brain region (for a total of n=8/group). Following electrophoresis, gels were activated with UV light (302nm) for 1 minute and then transferred onto polyvinyl-difluoride membranes (Bio-Rad) using the Trans-Blot Turbo Transfer System (Bio-Rad). Membranes were imaged for total protein using a ChemiDoc Imaging System (Bio-Rad, Mississauga, ON, CA), after which they were incubated for 1 hour at room temperature in a 5% non-fat milk solution in Tris-buffered saline solution with Tween-20 (TBS-T). Membranes were then incubated overnight at 4°C in anti-hevin antibody (host rabbit; 1:500; catalogue #: bs-6110R; Bioss) or anti-glypican 4/6 antibody (host rabbit; 1:500; catalogue #: 13048-1-AP; Proteintech, Rosemont, IL, USA) both in 5% non-fat milk/TBS-T, or anti-SPARC antibody (host goat; 0.4 µg/mL; catalogue #: AF942; R&D Systems) in 2% bovine serum albumin/TBS-T. Antibodies against hevin and SPARC recognized bands at ~130 kDa (Fig. 2G) and ~37 kDa (Fig. 3G) respectively. According to the manufacturer, the anti-glypican 4/6 antibody recognizes both cleaved (~35kDa) and full-length (~65kDa) glypican 4 and 6 (Proteintech). However, in our hands this antibody only detected the band at

~35 kDa, which corresponded to the cleaved proteins of glypican 4 and 6 and the one used in our analysis (Fig. 4C). Since the single band at ~35kDa represents both glypican 4 and 6, we will subsequently refer to this protein as GPC 4/6.

Following the incubation in primary antibody, membranes were washed 3 x 10 minutes in TBS-T at room temperature. Membranes were then incubated with horseradish peroxidase-conjugated secondary antibody against either rabbit (1:5000; catalogue #: NA934-1ML; GE Healthcare Life Sciences, Mississauga, ON, CA) or goat (1:5000; catalogue #: sc-2020; Santa Cruz Biotechnology, Santa Cruz, CA, USA) in 5% non-fat milk/TBS-T for hevin and GPC 4/6 detection, or TBS-T alone for SPARC detection, for 1 hour at room temperature. Membranes were washed again for 3 x 10 minutes in TBS-T, and developed using enhanced chemiluminescence (Bio-Rad). Membranes were scanned using a ChemiDoc Imaging System (Bio-Rad). Densitometry measurements were conducted using Image Lab Software 5.2 (Bio-Rad). Each band corresponding to either hevin (~130 kDa), SPARC (~37 kDa), or GPC 4/6 (~35 kDa) was first normalized to total protein within the same lane. These values were then expressed as a percentage of the average densitometry value obtained from the 4 WT samples within the same gel.

Table . Primary and secondary antibodies used for Western blotting. Antibody dilutions were optimized for use in Western Blotting.

Primary	Secondary
rabbit anti-hevin *(1:500; catalogue #: bs-6110R; Bioss)*	HRP-conjugated donkey anti-rabbit *(1:5000; catalogue #: NA934-1ML; GE Healthcare Life Sciences)*
goat anti-SPARC *(0.4 µg/mL; catalogue #: AF942; R&D Systems)*	HRP-conjugated donkey anti-goat *(1:5000; catalogue #: sc-2020; Santa Cruz Biotechnology)*
rabbit anti-glypican 4/6 *(1:500; catalogue #: 13048-1-AP; Proteintech)*	HRP-conjugated donkey anti-rabbit *(1:5000; catalogue #: NA934-1ML; GE Healthcare Life Sciences)*

3.4 Primary cortical astrocyte culture

Isolation and establishment of cortical astrocytes was carried out according to a protocol previously described by our laboratory (Jacobs and Doering, 2009). Cortical astrocytes were isolated from four WT or *Fmr1* KO pups at postnatal day (P)1 or P2 and grown in T75 tissue culture flasks in minimum essential media (Invitrogen, Carlsbad, CA, USA) supplemented with 6% glucose (Sigma-Aldrich) and 10% horse serum (Invitrogen). Cultures were maintained for approximately 1 week at 37°C and 5% CO_2. Cells were then removed from the T75 tissue culture flasks and re-plated onto coverslips coated with Poly-L-Lysine (Sigma-Aldrich, St. Louis, MO, USA; 1mg/mL) and laminin (Invitrogen; 0.1 mg/mL) at a density of 5000 cells per coverslip. Cells were maintained *in vitro* on coverslips for either 2 days, 1 week, or 2 weeks for subsequent immunocytochemical processing or for astrocyte-neuron co-culture and subsequent immunocytochemical processing.

3.5 Primary cortical astrocyte culture with MACS separation

Cortical tissue was isolated from 2 WT or *Fmr1* KO pups at P7 and cells were dissociated as described by Jacobs and Doering (2009). Of note, dissociation of cortical tissue from 2 P7 pups yields approximately 10^6 cells. Following tissue dissociation, cells were suspended in 80µl of PBS containing 0.5% BSA (pH 7.4). The cell suspension was blocked with an FcR blocking reagent (catalogue #: 130-097-678; Miltenyi Biotec, Bergisch Gladbach, Germany) and then magnetically labelled with Anti-ACSA-2 (astrocyte cell surface antigen-2) microbeads (catalogue #: 130-097-678; Miltenyi Biotec). The cell suspension was then washed with 2ml of PBS with 0.5% BSA and centrifuged at 200 x g for 10 minutes. Cells were then re-suspended in

500µl of PBS with 0.5% BSA. This cell suspension was then passed through a MACS MS column (Miltenyi Biotec) that was mounted within the magnetic field of a MACS separator (Miltenyi Biotec). The positive fraction containing magnetically-labelled cells was collected and plated into a T75 tissue culture flask with minimal essential media (Invitrogen) supplemented with 6% glucose (Sigma-Aldrich) and 10% horse serum (Invitrogen). Cultures were maintained for approximately 1 week at 37°C and 5% CO_2. Cells were then removed from the T75 tissue culture flasks and re-plated onto coverslips coated with Poly-L-Lysine (Sigma-Aldrich, St. Louis, MO, USA; 1mg/mL) and laminin (Invitrogen; 0.1 mg/mL) at a density of 5000 cells per coverslip. Cells were maintained *in vitro* on coverslips for either 1 or 2 weeks for subsequent immunocytochemical processing or for astrocyte-neuron co-culture and subsequent immunocytochemical processing.

3.6 Cortical and thalamic neuron cultures with MACS separation

WT or *Fmr1* KO cortical astrocytes that had previously been plated onto coverslips coated with Poly-L-Lysine (Sigma-Aldrich; 1mg/ml) and laminin (Invitrogen; 0.1 mg/mL) at a density of 5000 cells per coverslip were maintained for 2 days *in vitro* in minimal essential media (Invitrogen) supplemented with 6% glucose (Sigma-Aldrich) and 10% horse serum (Invitrogen). After 2 days this media was switched to neural maintenance media (NMM) composed of minimal essential media (Invitrogen) supplemented with 6% glucose (Sigma-Aldrich), 1% N2 supplement (Invitrogen), and 1mM sodium pyruvate (Invitrogen). The following day, cortical and thalamic tissue was isolated from 5-6 WT or *Fmr1* KO pups at P1. Cortical and thalamic tissue was dissociated using a neural tissue dissociation kit (catalogue #: 130-092-628; Miltenyi Biotec). Following dissociation cortical and thalamic cells were re-

suspended in 80µl of PBS with Mg^{2+} and Ca^{2+} and 0.5% BSA. Cells suspensions were then incubated with a non-neuronal cells biotin-antibody cocktail (catalogue #: 130-098-754; Miltenyi Biotec). Cell suspensions were then washed with PBS with Mg^{2+} and Ca^{2+} and 0.5% BSA and centrifuged for 200 x g for 10 minutes. Cells were re-suspended in 80µl of PBS with Mg^{2+} and Ca^{2+} and 0.5% BSA and magnetically labelled with anti-biotin microbeads (catalogue #: 130-098-754; Miltenyi Biotec). The volume of each cell suspension was adjusted to 500µl through the addition of PBS with Mg^{2+} and Ca^{2+} and 0.5% BSA. These cell suspensions were then passed twice through a MACS MS column (Miltenyi Biotec) that was mounted within the magnetic field of a MACS separator (Miltenyi Biotec). The negative fraction from each suspension, containing unlabeled cells, was collected and plated onto coverslips with the previously plated astrocytes (Fig. 3 and Table 1). Cells from each of the thalamic and cortical negative fractions were plated at a density of 10 000 cells per coverslip. Co-cultures were maintained in NMM for either 1 or 2 weeks at 37°C and 5% CO_2 for subsequent immunocytochemical processing.

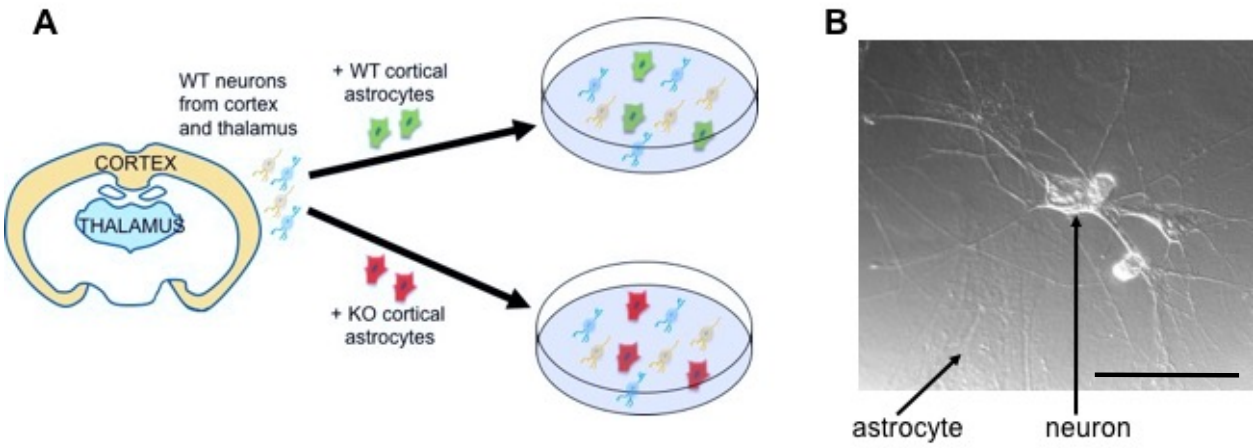
A
WT neurons
from cortex
and thalamus
CORTEX
THALAMUS
+ WT cortical
astrocytes
+ KO cortical
astrocytes
B
astrocyte
neuron

Figure 3. Schematic of plating combinations for astrocyte and neuron co-cultures. (A) Cortical and thalamic neurons were collected from WT pups and were plated in combination with either cortical astrocytes from WT pups or cortical astrocytes from KO pups. **(B)** Differential interface contrast image showing a co-culture containing both astrocytes and neurons. Image was obtained using a 60x objective with a Zeiss Axioimager. M2. Scale bar=50µm

Table 1. Plating combinations for astrocyte and neuron co-cultures. Thalamic and cortical neurons were collected from WT pups at postnatal day (P)1 and plated onto either WT or *Fmr1* KO cortical astrocytes collected from pups at either P1 or P7. Astrocyte-neuron co-cultures were maintained for either 7 or 14 days *in vitro*.

Co-culture group	Neurons	Astrocytes	Days *in vitro*
1	P1 thalamic and cortical, WT	P7, WT	14
2	P1 thalamic and cortical, WT	P7, KO	14
3	P1 thalamic and cortical, WT	P1, WT	14
4	P1 thalamic and cortical, WT	P1, KO	14
5	P1 thalamic and cortical, WT	P7, WT	7
6	P1 thalamic and cortical, WT	P7, KO	7
7	P1 thalamic and cortical, WT	P1, WT	7
8	P1 thalamic and cortical, WT	P1, KO	7

3.7 Immunocytochemistry

Astrocyte cultures were incubated in ice-cold acetone for 10 minutes, then permeabilized using 0.1% Triton X-100 (Sigma-Aldrich) for 5 minutes and placed in 1% bovine serum albumin (Sigma-Aldrich) in 0.01M phosphate-buffered saline for 1 hour at room temperature. After blocking, cells were incubated in primary antibodies (diluted in 0.01M phosphate-buffered saline) overnight at 4°C. The following antibodies were used to examine the distribution of hevin, SPARC, and GPC 4 in vitro: rabbit anti-glial fibrillary acidic protein (GFAP; 1:500; catalogue #: Z0334; Dako, Burlington, ON, CA), chicken anti-GFAP (1:2000; catalogue #: CH22102; Neuromics, Minneapolis, MN, USA) rabbit anti-hevin antibody (1:100; catalogue #: bs-6110R; Bioss, Woburn, MA, USA), goat anti-SPARC antibody (10 µg/mL; catalogue #: AF942; R&D Systems, Minneapolis, MN, USA), mouse anti-glypican 4 (1:50; catalogue #: GTX50007; GeneTex, Irvine, CA, USA). Cells were then incubated in secondary antibodies (in 0.01M phosphate-buffered saline) for 3 hours at room temperature. These included donkey anti-rabbit Alexa Flour 568 (1:200; catalogue #: A10042; Invitrogen), donkey anti-mouse Alexa Flour 594 (1:1000; catalogue #: A-21203; Invitrogen), donkey anti-goat FITC (1:100; catalogue #: 705-095-147; Jackson ImmunoResearch, West Grove, PA, USA), donkey anti-chicken FITC (1:100; catalogue #: 703-095-155; Jackson ImmunoResearch). Coverslips were mounted onto slides using ProLong Gold Antifade Mountant with 4', 6-diamidino-2-phenylindole (Life Technologies, Carlsbad, CA, USA). Two independent cultures (N=2) and a total of 50 cells (n=50) were examined per genotype. Images were acquired using a Zeiss AxioImager.M2 (Zeiss, Oberkochen, Germany) microscope.

In addition, Astrocyte and neuron co-cultures were also processed as described above in order to identify co-localized VGlut2^{+} pre-synaptic and PSD95^{+} post-synaptic puncta. The following primary and secondary antibodies were used: rabbit anti-vesicular glutamate transporter 2 (VGlut2; 1:500; catalogue #: 135 403; Synaptic Systems, Göttingen, Germany), mouse anti-post-synaptic density protein 95 (PSD95; 1:100; catalogue #: MAB1596; Millipore), rabbit anti-GFAP (1:500; catalogue #: Z0334; Dako, Burlington, ON, CA), chicken anti-microtubule associated protein 2 (MAP2; 1:1000; catalogue #: CH22103; Neuromics, Minneapolis, MN, USA), goat anti-rabbit FITC (1:100; catalogue #: 111-095-144; Jackson ImmunoResearch), donkey anti-mouse Alexa Flour 594 (1:1500; catalogue #: A-21203; Invitrogen), donkey anti-rabbit Alexa Flour 568 (1:200; catalogue #: A10042; Invitrogen), donkey anti-chicken FITC (1:100; catalogue #: 703-095-155; Jackson ImmunoResearch). One independent culture (N=1) and a total of 10 neurons (n=10) were examined per condition.

Table . Primary and secondary antibodies used for immunocytochemistry. Antibody dilutions were optimized for use in astrocyte cultures and astrocyte-neuron co-cultures.

Primary 1	Secondary 1	Primary 2	Secondary 2
rabbit anti-hevin *(1:100; catalogue #: bs-6110R; Bioss)*	donkey anti-rabbit Alexa Flour 568 *(1:200; catalogue #: A10042; Invitrogen)*	chicken anti-GFAP *(1:2000; catalogue #: CH22102; Neuromics)*	donkey anti-chicken FITC *(1:100; catalogue #: 703-095-155; Jackson ImmunoResearch)*
goat anti-SPARC *(10 µg/mL; catalogue #: AF942; R&D Systems)*	donkey anti-goat FITC *(1:100; catalogue #: 705-095-147; Jackson ImmunoResearch)*	rabbit anti-GFAP *(1:500; catalogue #: Z0334; Dako)*	donkey anti-rabbit Alexa Flour 568 *(1:200; catalogue #: A10042; Invitrogen)*
mouse anti-glypican 4 *(1:50; catalogue #: GTX50007; GeneTex)*	donkey anti-mouse Alexa Flour 594 *(1:1000; catalogue #: A-21203; Invitrogen)*	chicken anti-GFAP *(1:2000; catalogue #: CH22102; Neuromics)*	donkey anti-chicken FITC *(1:100; catalogue #: 703-095-155; Jackson ImmunoResearch)*
chicken anti-MAP2 *(1:1000; catalogue #: CH22103; Neuromics)*	donkey anti-chicken FITC *(1:100; catalogue #: 703-095-155; Jackson ImmunoResearch)*	rabbit anti-GFAP *(1:500; catalogue #: Z0334; Dako)*	donkey anti-rabbit Alexa Flour 568 *(1:200; catalogue #: A10042; Invitrogen)*
rabbit anti-VGlut2 *(1:500; catalogue #: 135 403; Synaptic Systems)*	goat anti-rabbit FITC *(1:100; catalogue #: 111-095-144; Jackson ImmunoResearch)*	mouse anti-PSD95 *(1:100; catalogue #: MAB1596; Millipore)*	donkey anti-mouse Alexa Flour 594 *(1:1500; catalogue #: A-21203; Invitrogen)*

3.8 Synaptic puncta analysis

Images were obtained using a Zeiss AxioImager.M2 (Zeiss, Oberkochen, Germany) microscope with Zeiss Zen Blue Imaging Software. SynapCountJ, a custom written plug-in for ImageJ (National Institutes of Health, Bethesda, MD, USA) was used to identify co-localized puncta. Thalamocortical synapse candidates were identified by the co-localization of presynaptic VGlut2^{+} and postsynaptic PSD95^{+} puncta. Cortical neurons were imaged, while thalamic neurons were avoided by the presence of intense VGlut2^{+} staining within the cell body. For each condition, 10 cortical neurons (n=10) were randomly selected across two coverslips from one culture (N=1). Low frequency background was removed from both the red and green channels of each image using the ImageJ rolling ball background subtraction algorithm. The dendrites of a neuron were traced using the ImageJ plugin NeuronJ. The coordinates of these tracings were uploaded into SynapCountJ along with the corresponding red and green channel images. The number of colocalized puncta was measured for each tracing and normalized to the tracing length.

3.9 Statistical analyses

Statistical analysis was conducted using GraphPad Prism Software 5.0 (GraphPad Software Inc., San Diego, CA, USA). Unpaired, two-tailed t-tests were used to determine significant differences, using Welch's correction when required, and all results are shown as mean ± SEM. Probability values < 0.05 were considered statistically significant.

CHAPTER FOUR

RESULTS

In this study, we investigated the *in vivo* levels of hevin, SPARC and GPC 4/6 in the cortical and hippocampal brain regions of WT and *Fmr1* KO mice at ages P7, P14, and P21. Importantly, these factors are secreted by astrocytes and are known to be involved in synapse development and maturation. In FXS, distorted dendritic spine morphology has been revealed within the hippocampus and cortex (Antar et al., 2006; Cruz-Martin et al., 2010; Irwin et al., 2001), indicating abnormal development of excitatory connections with in these brain regions. We hypothesized that there may be altered levels of astrocyte-derived hevin, SPARC, and/or GPC 4/6 in *Fmr1* KO mice, indicative of aberrant astrocyte-signalling in the FXS brain. Protein expression of GPC 4/6 did not vary between the genotypes at all time-points examined. However, we did find altered protein levels of hevin and SPARC in *Fmr1* KO mice compared to that of WT mice. While the distribution of both proteins in astrocytes *in vitro* appears consistent across the two genotypes, the overall dysregulation of these factors in *Fmr1* KO mice suggests that they play a role in the altered neurobiology of FXS.

4.1 Hevin and SPARC protein levels are altered in the cortex of *Fmr1* KO mice, relative to WT mice.

Hevin was highly expressed in primary cortical astrocytes cultured from both WT and *Fmr1* KO mice, and showed a similar distribution pattern between the genotypes (N=2, n=50; Fig. 1A). Western blotting revealed a genotypic difference in hevin levels in cortical tissue from P14 mice. The *Fmr1* KO group showed significantly higher hevin levels than the WT group (*Fmr1* KO 144.50 ± 13.36% of WT; n=8/group; $P < 0.05$; Fig. 1B, D). Interestingly, there were no differences between WT and *Fmr1* KO groups at either P7 (*Fmr1* KO 81.92 ± 16.35% of

WT; n=8/group; Fig. 1C) or P21 (*Fmr1* KO 103.80 ± 11.33% of WT; n=8/group; Fig. 1E) in the cortex.

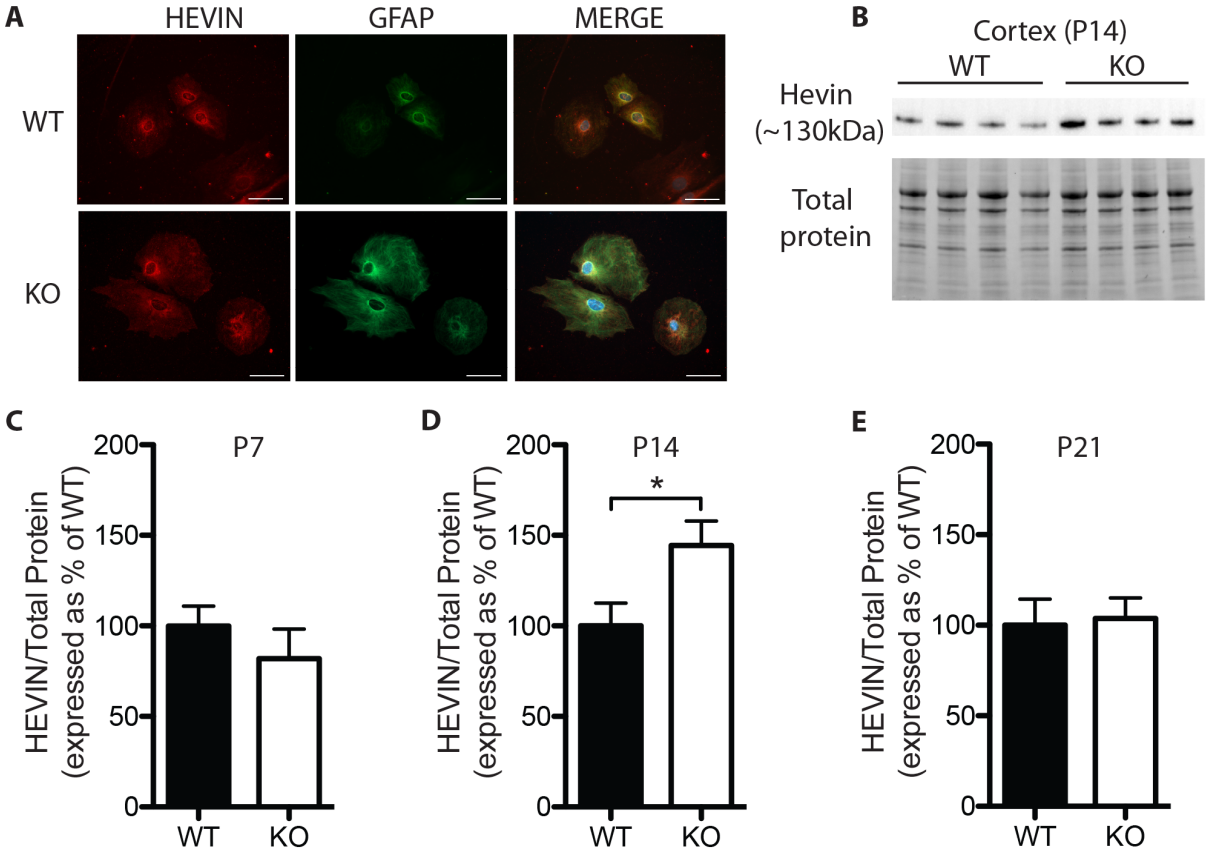
A
HEVIN
GFAP
MERGE
WT
KO
B
Cortex (P14)
WT
KO
Hevin
(~130kDa)
Total
protein
C
P7
HEVIN/Total Protein
(expressed as % of WT)
200
150
100
50
0
WT
KO
D
P14
*
HEVIN/Total Protein
(expressed as % of WT)
200
150
100
50
0
WT
KO
E
P21
HEVIN/Total Protein
(expressed as % of WT)
200
150
100
50
0
WT
KO

Figure 4. Hevin expression is altered at postnatal day (P)14 in the cortex of *Fmr1* KO mice. **(A)** Cultured cortical astrocytes co-labelled with anti-glial fibrillary acidic protein (GFAP; green) and anti-hevin (red) after 2 days *in vitro.* Nuclei were stained with 4', 6-diamidino-2-phenylindole (blue). Images were obtained using a 40x objective with a Zeiss Axioimager. M2. Scale bars=50μm. **(B)** A representative western blot showing hevin (~130 kDa) in cortical samples (30μg of protein per lane) from P14 WT and *Fmr1* KO mice, as well as several bands corresponding the total protein within each lane. **(C-E)** Hevin expression in the cortex of WT (black; n=8) and *Fmr1* KO (white; n=8) mice at P7, P14, and P21. Bands representing hevin were normalized against the total protein within the same lane on the membrane, and were then expressed as a percent of the average level of hevin in the WT group. (*$P < 0.05$)

In cultured cortical astrocytes, SPARC was similarly expressed between genotypes at 2 days *in vitro* (N=2, n=50; Fig. 2A). A representative Western blot showing SPARC (~37 kDa) from WT and *Fmr1* KO cortical samples collected at P14 is shown in Fig. 2B. Similar to our finding with hevin, genotypic differences were evident at the different developmental time-points. In the cortex, at P7 and P14, the *Fmr1* KO group had lower SPARC levels than the WT group (*Fmr1* KO 85.72 ± 5.88% and 84.88 ± 4.31% of WT, respectively; n=8/group; $P < 0.05$ for both comparisons; Fig. 2C and 2D). No significant difference was observed between WT and *Fmr1* KO groups at P21 (*Fmr1* KO 94.65 ± 3.87% of WT; n=8/group; Fig. 3F). Thus, cortical levels of hevin and SPARC displayed genotypic differences at specific developmental time-points, suggesting that altered expression of these factors during certain developmental windows may contribute to mechanisms underlying aberrant synapse development in FXS.

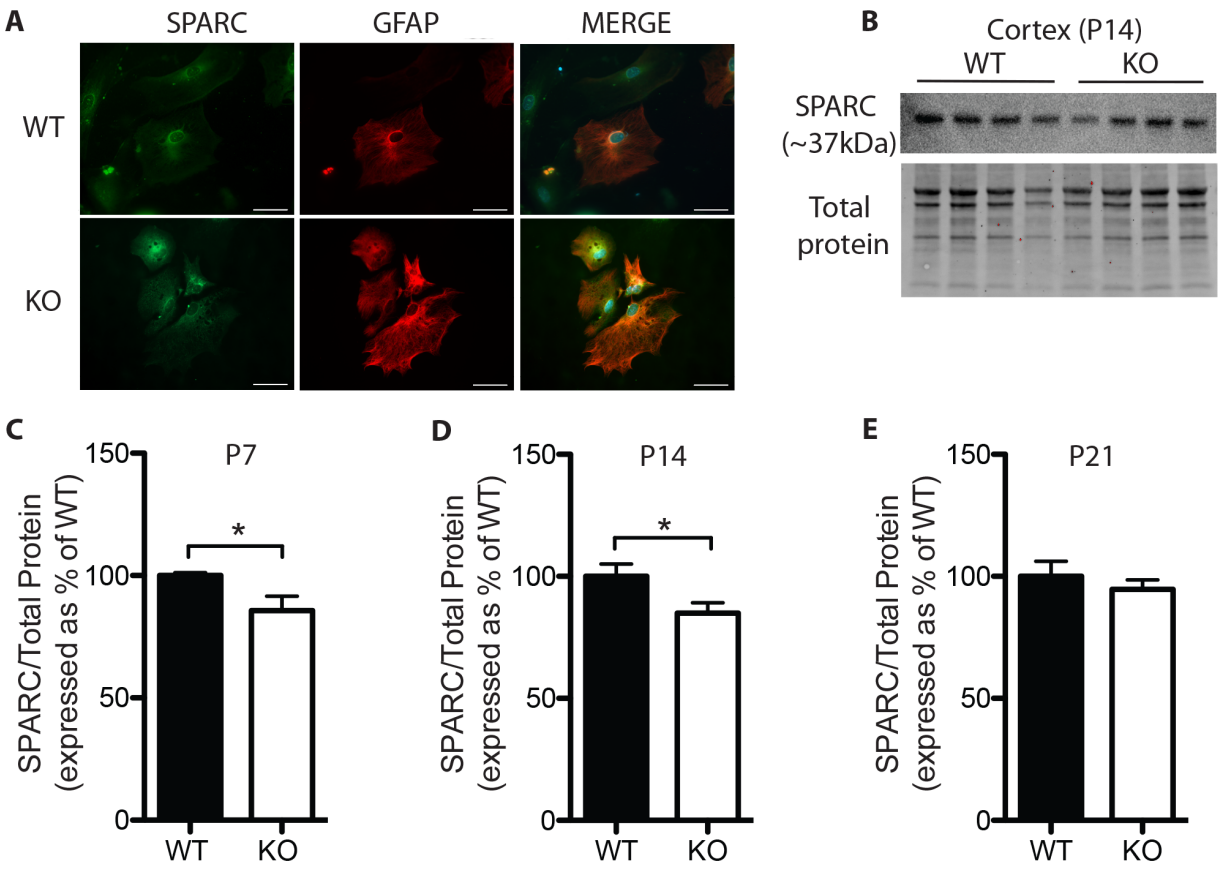
A
SPARC
GFAP
MERGE
WT
KO
B
Cortex (P14)
WT
KO
SPARC
(~37kDa)
Total
protein
C
P7
SPARC/Total Protein
(expressed as % of WT)
150
100
50
0
*
WT
KO
D
P14
SPARC/Total Protein
(expressed as % of WT)
150
100
50
0
*
WT
KO
E
P21
SPARC/Total Protein
(expressed as % of WT)
150
100
50
0
WT
KO

Figure 5. SPARC expression is altered at postnatal day (P)7 and P14 in the cortex of *Fmr1* KO mice. (A) Cultured cortical astrocytes co-labelled with anti-glial fibrillary acidic protein (GFAP; red) and anti-SPARC (green) after 2 days *in vitro.* Nuclei were stained with 4', 6-diamidino-2-phenylindole (blue). Images were obtained using a 40x objective with a Zeiss Axioimager. M2. Scale bars=50 μm. **(B)** A representative western blot shows bands at ~37 kDa corresponding to SPARC in cortical samples (30μg of protein per lane) from P14 WT and *Fmr1* KO mice, as well as the total protein within each lane. **(C-E)** SPARC expression in the cortex of WT (black, n=8) and *Fmr1* KO (white, n=8) mice at P7, P14, and P21. Bands representing SPARC were normalized against the total protein within the same lane on the membrane, and were then expressed as a percent of the average level of SPARC in the WT group. (*$P < 0.05$)

4.2 Hevin protein levels, but not SPARC levels, are altered in the hippocampus of *Fmr1* KO mice, relative to WT mice.

Levels of hevin in the hippocampus differed between WT and *Fmr1* KO mice; however, these alterations were notably different than those found in the cortex. Bands representing hevin in hippocampal samples from P7 WT and *Fmr1* KO mice are shown in a Western blot in Fig. 3A. At this time-point, the *Fmr1* KO group showed significantly lower hevin levels than the WT group (*Fmr1* KO 31.41 ± 6.86% of WT; $P < 0.0005$; n=8/group; Fig. 3B). At P14 there was no significant difference in hevin levels between *Fmr1* KO and WT groups (*Fmr1* KO 89.80 ± 21.03 % of WT; n=8/ group; Fig. 3C), and at age P21, the *Fmr1* KO group had significantly higher hevin levels than the WT group (*Fmr1* KO 145.70 ± 15.17% of WT; n=8/group; $P < 0.05$; Fig. 3D).

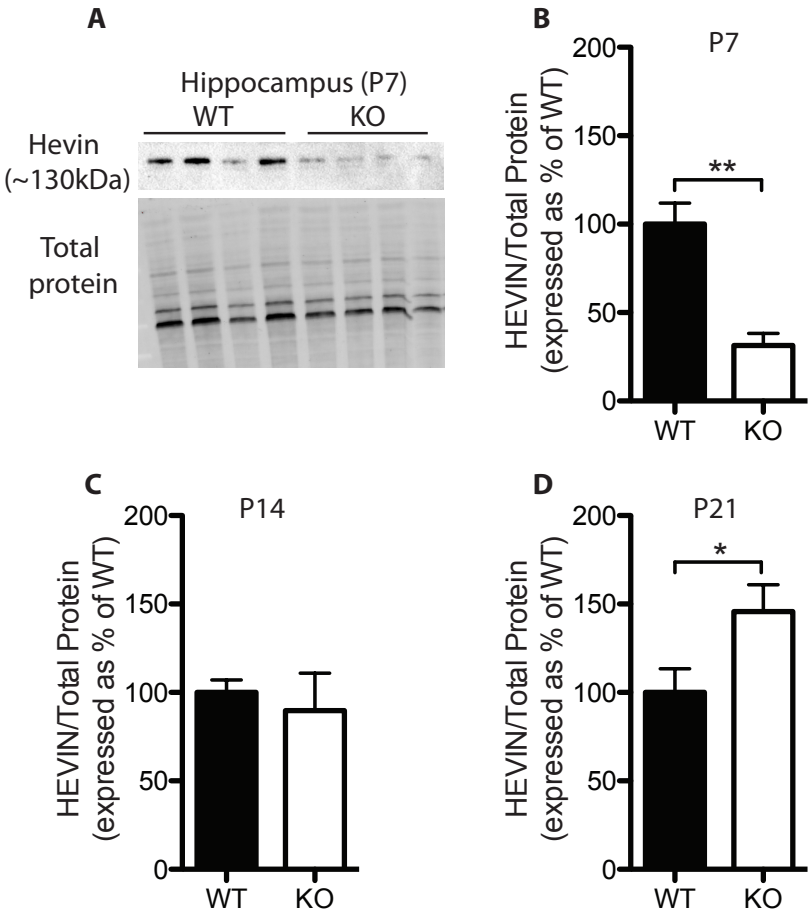
A
Hippocampus (P7)
WT
KO
Hevin
(~130kDa)
Total
protein
B
P7
HEVIN/Total Protein
(expressed as % of WT)
200
150
100
50
0
**
WT
KO
C
P14
HEVIN/Total Protein
(expressed as % of WT)
200
150
100
50
0
WT
KO
D
P21
HEVIN/Total Protein
(expressed as % of WT)
200
150
100
50
0
*
WT
KO

Figure 6. Hevin expression is altered at postnatal day (P)7 and P21 in the hippocampus of *Fmr1* KO mice. (A) A representative western blot shows hevin (~130 kDa) in hippocampal samples (30μg of protein per lane) from P7 WT and *Fmr1* KO mice, as well as the total protein within each lane. **(B-D)** Hevin expression in the hippocampus of WT (black; n=8) and *Fmr1* KO (white; n=8) mice at P7, P14, and P21. Bands representing hevin were normalized against the total protein within the same lane on the membrane, and were then expressed as a percent of the average level of hevin in the WT group. (*$P < 0.05$, ** $P < 0.0005$)

A representative Western blot showing SPARC from WT and *Fmr1* KO P7 hippocampal samples is shown in Fig. 4A. In contrast to our findings with hevin expression, there were no significant differences in hippocampal SPARC levels between WT and *Fmr1* KO mice at P7 (*Fmr1* KO 107.60 ± 4.99% of WT; n=8/group; Fig. 4B), P14 (*Fmr1* KO 124.10 ± 12.94% of WT; n=8/group; Fig. 4C), or P21 (*Fmr1* KO 90.86 ± 3.26% of WT; n=8/group; Fig. 4D).

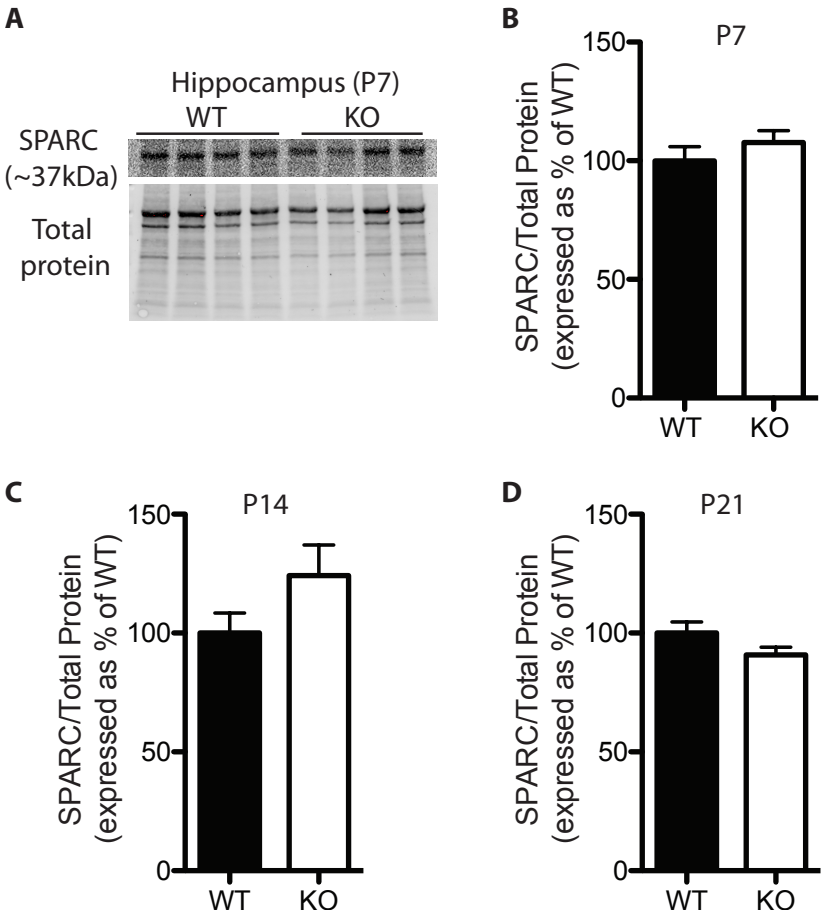
A
Hippocampus (P7)
WT
KO
SPARC
(~37kDa)
Total
protein
B
P7
SPARC/Total Protein
(expressed as % of WT)
150
100
50
0
WT
KO
C
P14
SPARC/Total Protein
(expressed as % of WT)
150
100
50
0
WT
KO
D
P21
SPARC/Total Protein
(expressed as % of WT)
150
100
50
0
WT
KO

Figure 7. SPARC expression is not significantly altered in the hippocampus of *Fmr1* KO mice. (A) A representative western blot with bands at ~37 kDa corresponding to SPARC in hippocampal samples (30µg of protein per lane) from postnatal day (P)7 WT and *Fmr1* KO mice, as well as the total protein within each lane. **(B-D)** SPARC expression in the hippocampus of WT (black, n=8) and *Fmr1* KO (white, n=8) mice at P7, P14, and P21. Bands representing SPARC were normalized against the total protein within the same lane on the membrane, and were then expressed as a percent of the average level of SPARC in the WT group.

4.3 GPC 4/6 protein levels in *Fmr1* KO mice did not differ significantly from WT mice.

GPC 4/6 was similarly expressed in both WT and *Fmr1* KO cultured cortical astrocytes *in vitro* (N=2, n=50; Fig. 5A). Due to the relatively low expression of GPC 4/6 in the mouse brain at P7 and P14, we were unable to detect or compare protein levels in the samples from these time points via Western blotting. Representative Western blots displaying bands corresponding to GPC 4/6 (~35 kDa) from WT and *Fmr1* KO P21 cortical samples and hippocampal samples are shown in Fig. 5B and 5D, respectively. At P21, there were no significant differences in GPC 4/6 levels between *Fmr1* KO and WT groups in the cortex (*Fmr1* KO 65.06 ± 14.17% of WT; n=8/group; Fig. 5C) or hippocampus (*Fmr1* KO 104.7 ± 10.15% of WT; n=8/group; Fig. 5E).

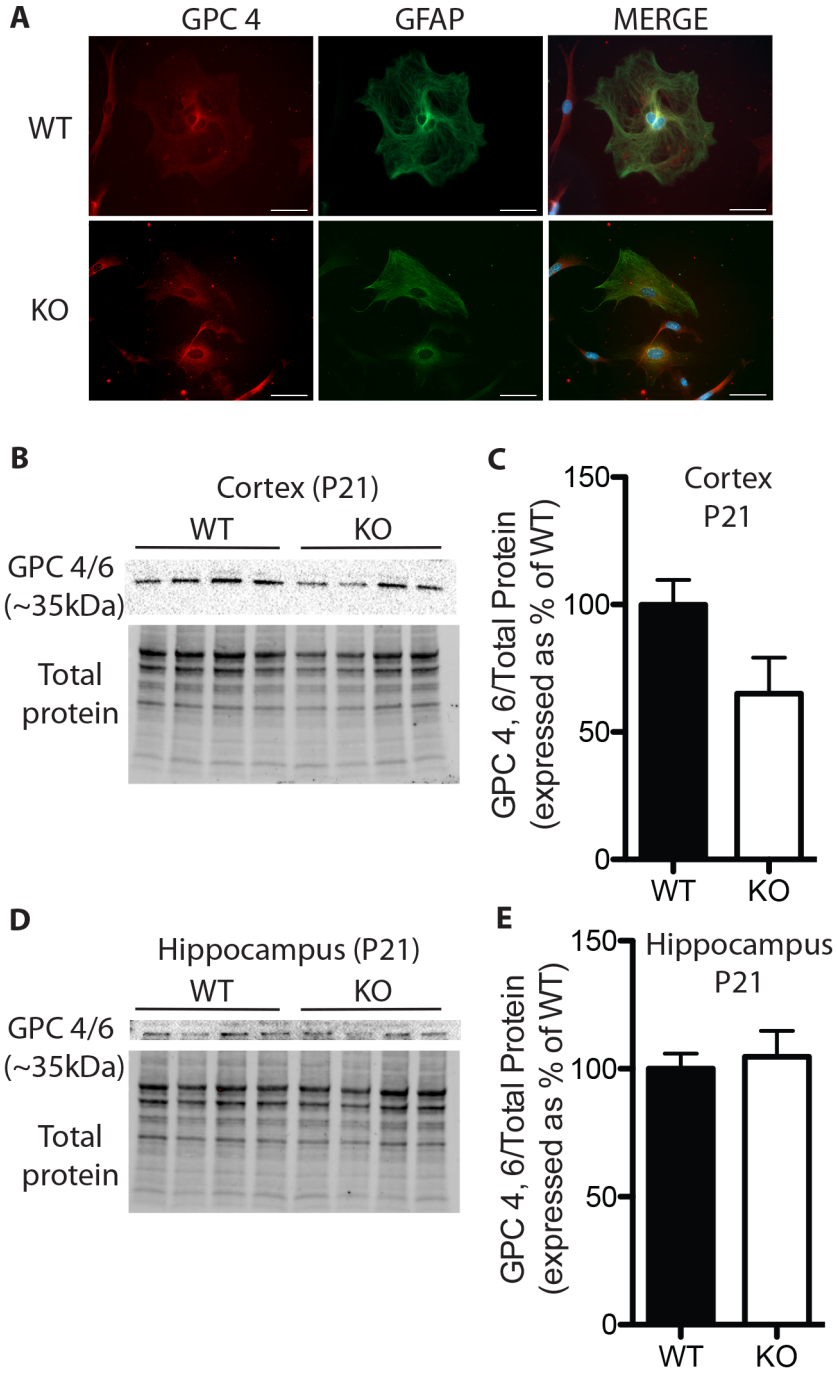
A
GPC 4
GFAP
MERGE
WT
KO
B
Cortex (P21)
WT
KO
GPC 4/6
(~35kDa)
Total
protein
C
Cortex
P21
GPC 4, 6/Total Protein
(expressed as % of WT)
150
100
50
0
WT
KO
D
Hippocampus (P21)
WT
KO
GPC 4/6
(~35kDa)
Total
protein
E
Hippocampus
P21
GPC 4, 6/Total Protein
(expressed as % of WT)
150
100
50
0
WT
KO

Figure 8. GPC 4/6 expression is not significantly altered in *Fmr1* KO mice at postnatal day (P)21. (A) Cultured cortical astrocytes co-labelled with anti-glial fibrillary acidic protein (GFAP; green) and anti-GPC4 (red) after 2 days *in vitro.* Nuclei were stained with 4', 6-diamidino-2-phenylindole (blue). Images were obtained using a 40x objective with a Zeiss Axioimager. M2. Scale bars=50 μm. **(B)** A representative western blot shows bands at ~35 kDa corresponding to GPC 4/6 in cortical samples (50μg of protein per lane) from WT and *Fmr1* KO mice at P21, as well as the total protein within each lane. Bands representing GPC 4/6 were normalized against the total protein within the same lane on the membrane. **(C)** GPC 4/6 expression in the cortex of WT (black, n=8) and *Fmr1* KO (white, n=8) mice at P21. *Fmr1* KO GPC 4/6 protein levels were expressed as a percent of the average level of GPC 4/6 in the WT group. **(D)** A representative western blot with bands corresponding to GPC 4/6 in hippocampal samples (50μg of protein per lane) from WT and *Fmr1* KO mice at P21, as well as the total protein within each lane. **(E)** GPC 4/6 expression in the hippocampus of WT (black, n=8) and *Fmr1* KO (white, n=8) mice at P21.

4.4 The number of Vglut2^{+}/ PSD95^{+} co-localized puncta is increased in co-cultures of *Fmr1* KO astrocytes and WT neurons, compared to co-cultures of WT astrocytes and WT neurons.

Thalamic and intracortical axonal projections that contact dendritic spines make up the majority of excitatory synapses in the cortex, and these two inputs can be distinguished by their vesicular glutamate transporter-2 (VGlut2) or vesicular glutamate transporter-1 (VGlut1) contents, respectively (Fremeau et al., 2001; Kaneko and Fujiyama, 2002; Graziano et al., 2008). Hevin is necessary for the formation of thalamocortical excitatory synapses (Risher et al., 2014; Singh et al., 2016) and we found an increase in the cortical protein expression of hevin in P14 *Fmr1* KO mice, relative to WT mice. Therefore, we sought to determine whether there is a difference in the number of thalamocortical synapses that are formed in co-cultures of either WT astrocytes with WT thalamic and cortical neurons or KO astrocytes with WT thalamic and cortical neurons. Remaining cognizant of the differences between *in vivo* and *in vitro* systems we isolated astrocytes from pups at two different ages, P1 and P7, to determine if any differences arise when astrocytes are allowed to mature in vivo for an additional week. We employed MACS separation to isolate astrocytes from P7 pups and neurons from P1 pups and subsequently plated these cells to obtain astrocyte and neuron co-cultures (Fig. 9 & 10).

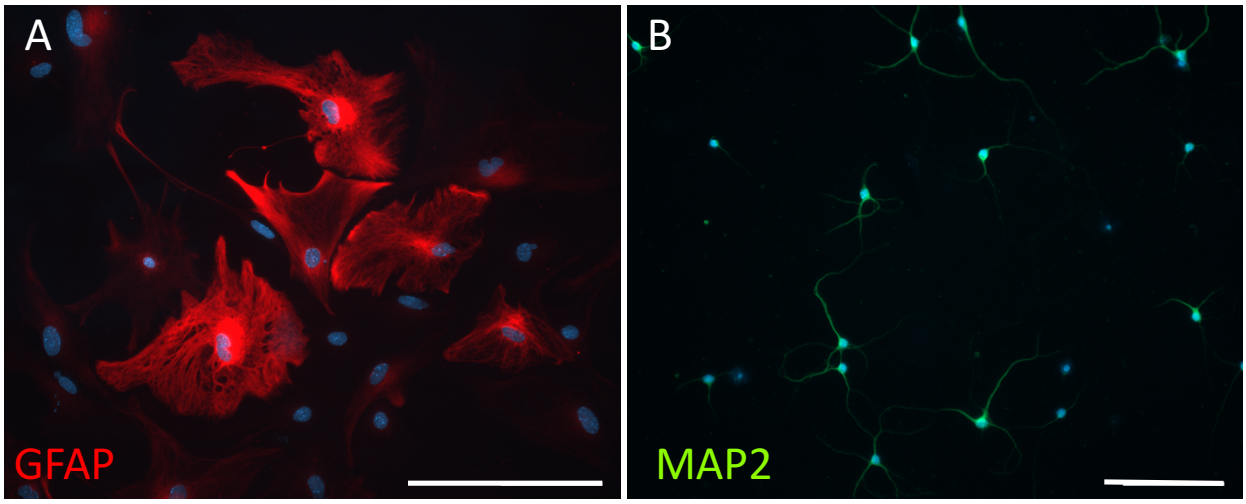
A
GFAP
B
MAP2

Figure 9. Astrocyte and neuron cultures following MACS separation. (A) Astrocyte culture following MACS separation. Astrocytes were isolated from P7 pups. **(B)** Neuron culture following MACS separation. Neurons were isolated from P1 pups and passed twice through a MACS MS column. Astrocyte and neuron cultures were each maintained for 2 days *in vitro*. Cultures were labelled with anti-glial fibrillary acidic protein (GFAP; red) and anti-microtubule associated protein 2 (MAP2; green) to visualize astrocytes and neurons, respectively. Images were obtained using a 20x objective with a Zeiss Axioimager. M2. Scale bars=100 μm.

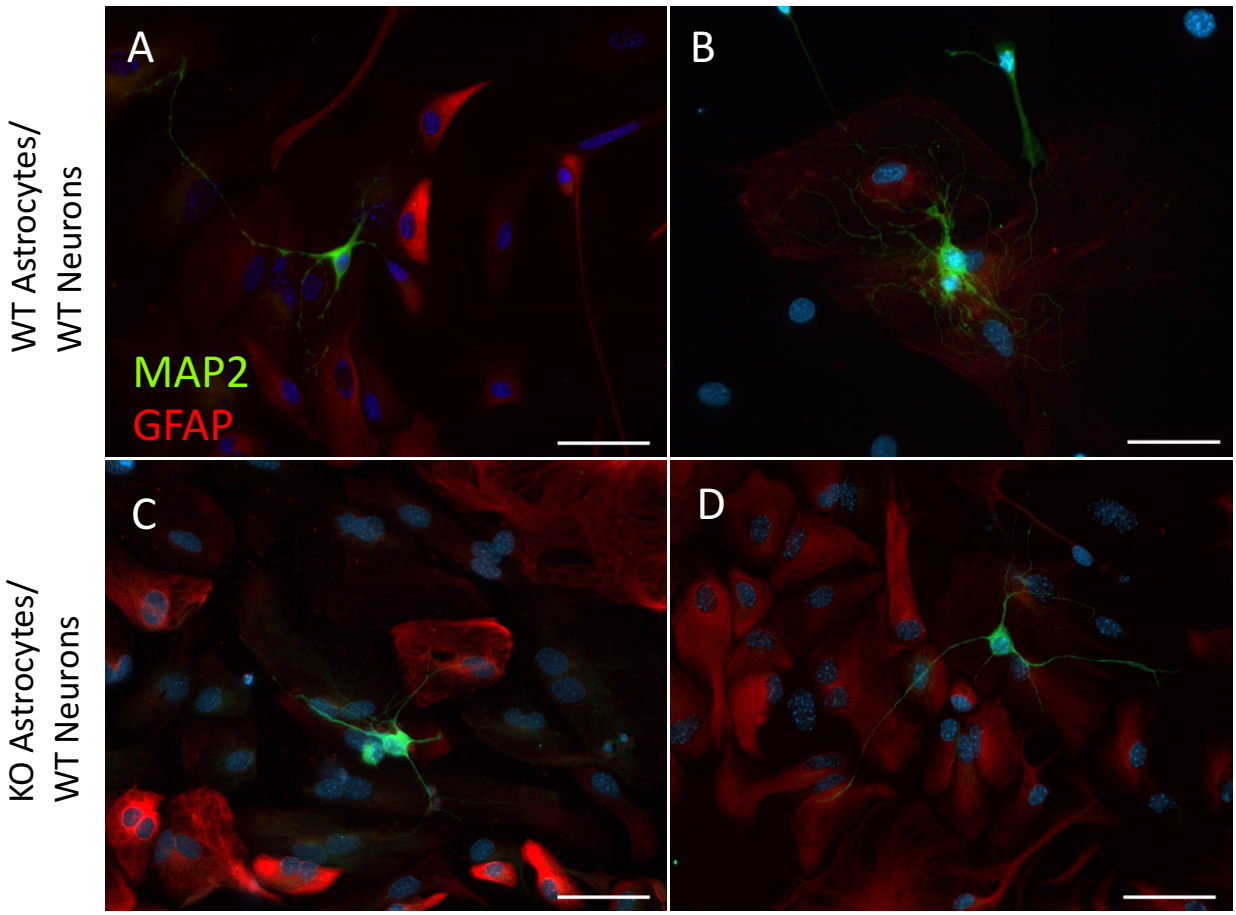
A
B
C
D
MAP2
GFAP
WT Astrocytes/
WT Neurons
KO Astrocytes/
WT Neurons

Figure 10. Astrocyte and neuron co-cultures. (A) WT neurons isolated from P1 pups via MACS separation were plated onto previously plated WT astrocytes isolated from P1 pups. **(B)** WT neurons isolated from P1 pups via MACS separation were plated onto previously plated WT astrocytes isolated via MACS separation from P7 pups. **(C)** WT neurons isolated from P1 pups via MACS separation were plated onto previously plated *Fmr1* KO astrocytes isolated from P1 pups. **(D)** WT neurons isolated from P1 pups via MACS separation were plated onto previously plated *Fmr1* KO astrocytes isolated via MACS separation from P7 pups. Co-cultures were maintained for 14 days *in vitro*. Co-cultures were labelled with anti-glial fibrillary acidic protein (GFAP; red) and anti-microtubule associated protein 2 (MAP2; green) to visualize astrocytes and neurons, respectively. Images were obtained using a 40x objective with a Zeiss Axioimager. M2. Scale bars=50 μm.

Excitatory thalamocortical synaptic candidates were identified by the colocalization of $VGlut2^{+}$ and $PSD95^{+}$ puncta. When WT cortical and thalamic neurons were cultured with *Fmr1* KO astrocytes (isolated from P7 pups) and maintained for 7 DIV, we found a trend, although non-significant, towards an increase in the number of thalamocortical synapses, relative to the number of thalamocortical synapses established in co-cultures of WT astrocytes and WT neurons (*Fmr1* KO astrocytes/ WT neurons: 18.07 ± 7.89; WT astrocytes/WT neurons: 5.76 ± 2.02; N=1, n=10/group; Fig.11). In co-cultures maintained for 14 DIV we found a significant increase in the number of thalamocortical synapses when *Fmr1* KO astrocytes (isolated from P7 pups) were grown with WT neurons, relative to WT astrocytes grown with WT neurons (*Fmr1* KO astrocytes/ WT neurons: 58.71 ± 13.45; WT astrocytes/ WT neurons: 24.49 ± 5.35; N=1, n=10/group; $P < 0.05$; Fig. 12). We observed similar results when astrocytes were isolated from P1 pups and cultured with cortical and thalamic neurons. Co-cultures of *Fmr1* KO astrocytes (isolated from P1 pups) and WT neurons that were maintained for 7 DIV showed an increased number of thalamocortical synapses, compared to WT astrocytes grown with WT neurons (*Fmr1* KO astrocytes/WT neurons: 18.02 ± 4.16; WT astrocytes/WT neurons: 6.55 ± 1.49; N=1, n=10/group; $P < 0.05$; Fig. 13A). After 14 DIV, we found a trend towards an increase in the number of thalamocortical synapses in co-cultures consisting of *Fmr1* KO astrocytes (isolated from P1 pups) and WT neurons, compared to co-cultures of WT astrocytes and WT neurons; However, this difference did not reach statistical significance (*Fmr1* KO astrocytes/ WT neurons: 28.03 ± 10.76; WT astrocytes/ WT neurons: 13.05 ± 2.21; N=1, n=10/group; Fig. 13B).

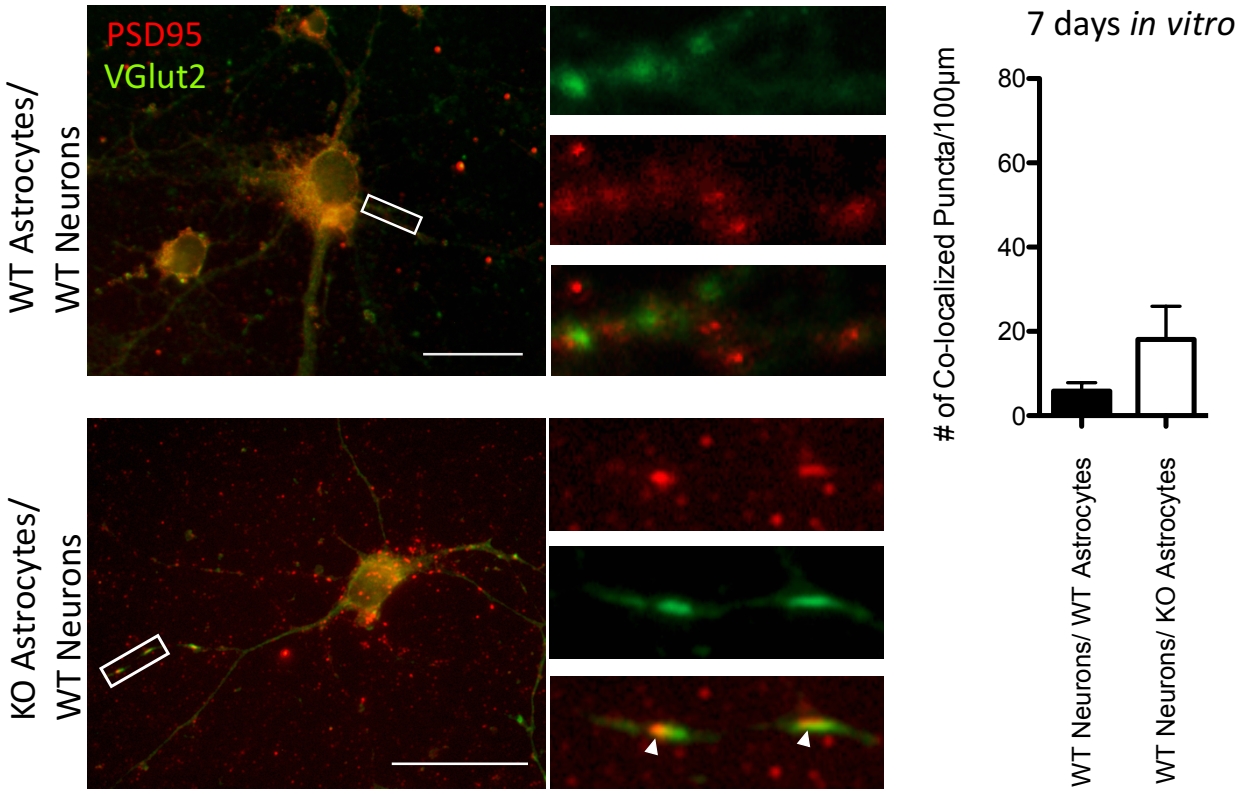
PSD95
VGlut2
WT Astrocytes/
WT Neurons
KO Astrocytes/
WT Neurons
7 days *in vitro*
# of Co-localized Puncta/100µm
80
60
40
20
0
WT Neurons/ WT Astrocytes
WT Neurons/ KO Astrocytes

Figure 11. VGlut2^{+}/ PSD95^{+} co-localized puncta in co-cultures of WT neurons with either WT or *Fmr1* KO astrocytes (isolated from P7 pups), maintained for 7 *DIV*. WT cortical and thalamic neurons were isolated from P1 pups via MACS separation and co-cultured with either WT or *Fmr1* KO astrocytes isolated from P7 pups via MACS separation. Co-cultures were maintained for 7 days *in vitro* and subsequently co-labelled with antibodies against vesicular glutamate transporter-2 (VGlut2) and post-synaptic density protein 95 (PSD95) to visualize pre-synaptic and post-synaptic puncta, respectively. White arrows indicate co-localized Vglut2^{+} (green) and PSD95^{+} (red) puncta. Measures of thalamocortical synapse number (identified by the co-localized VGlut2^{+} and PSD95^{+} puncta) were obtained from cultures containing WT astrocytes (black; N=1, n=10) and cultures containing *Fmr1* KO astrocytes (white; N=1, n=10) and normalized to dendrite length. Images were obtained using a 40x objective with a Zeiss Axioimager. M2. Scale bars=25 μm.

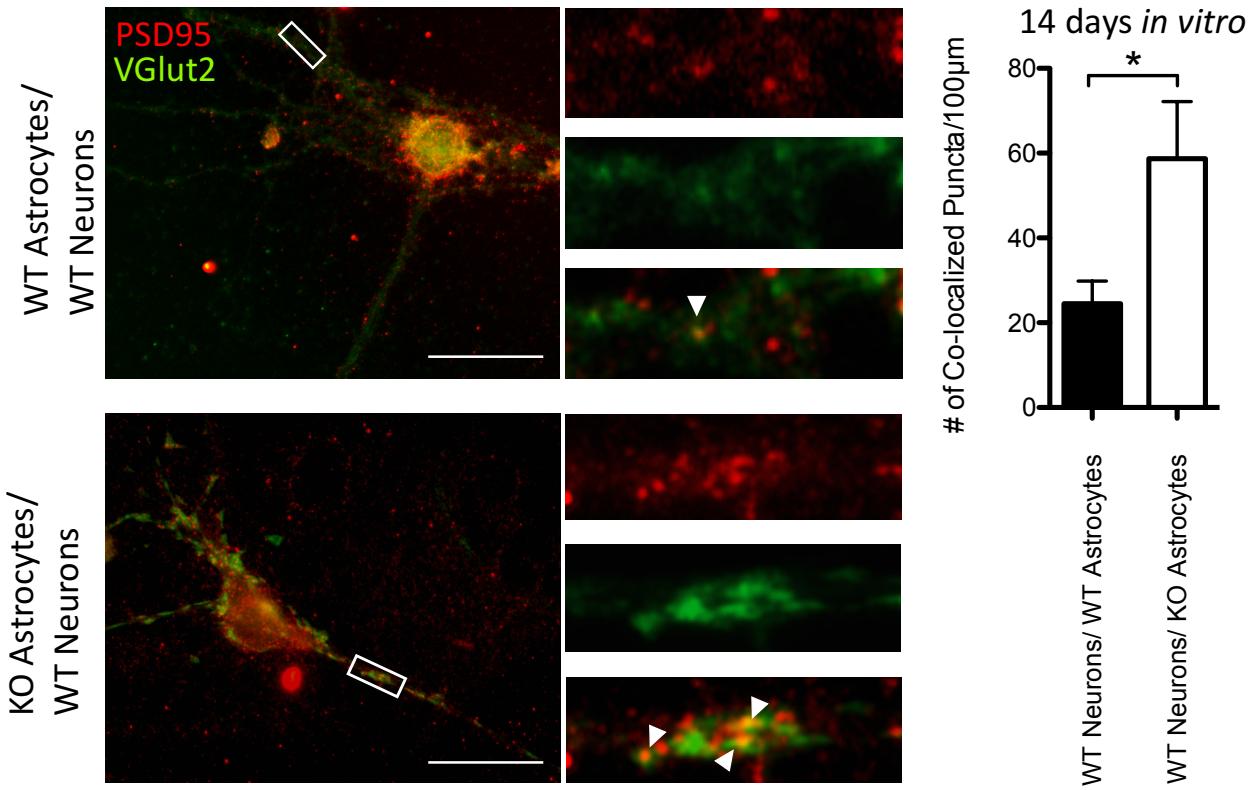
PSD95
VGlut2
WT Astrocytes/
WT Neurons
KO Astrocytes/
WT Neurons
14 days *in vitro*
# of Co-localized Puncta/100µm
80
60
40
20
0
*
WT Neurons/ WT Astrocytes
WT Neurons/ KO Astrocytes

Figure 12. At 14 *DIV* the number of VGlut2$^+$/ PSD95$^+$ co-localized puncta is increased in co-cultures of *Fmr1* KO astrocytes (isolated from P7 pups) and WT neurons, relative to co-cultures of WT astrocytes and WT neurons. WT cortical and thalamic neurons were isolated from P1 pups via MACS separation and co-cultured with either WT or *Fmr1* KO astrocytes isolated from P7 pups via MACS separation. Co-cultures were maintained for 14 days *in vitro* and subsequently co-labelled with antibodies against vesicular glutamate transporter-2 (VGlut2) and post-synaptic density protein 95 (PSD95) to visualize pre-synaptic and post-synaptic puncta, respectively. White arrows indicate co-localized Vglut2$^+$ (green) and PSD95$^+$ (red) puncta. Measures of thalamocortical synapse number (identified by the co-localized VGlut2$^+$ and PSD95$^+$ puncta) were obtained from cultures containing WT astrocytes (black; N=1, n=10) and cultures containing *Fmr1* KO astrocytes (white; N=1, n=10) and normalized to dendrite length. Images were obtained using a 40x objective with a Zeiss Axioimager. M2. Scale bars=25 μm. (*$P < 0.05$)

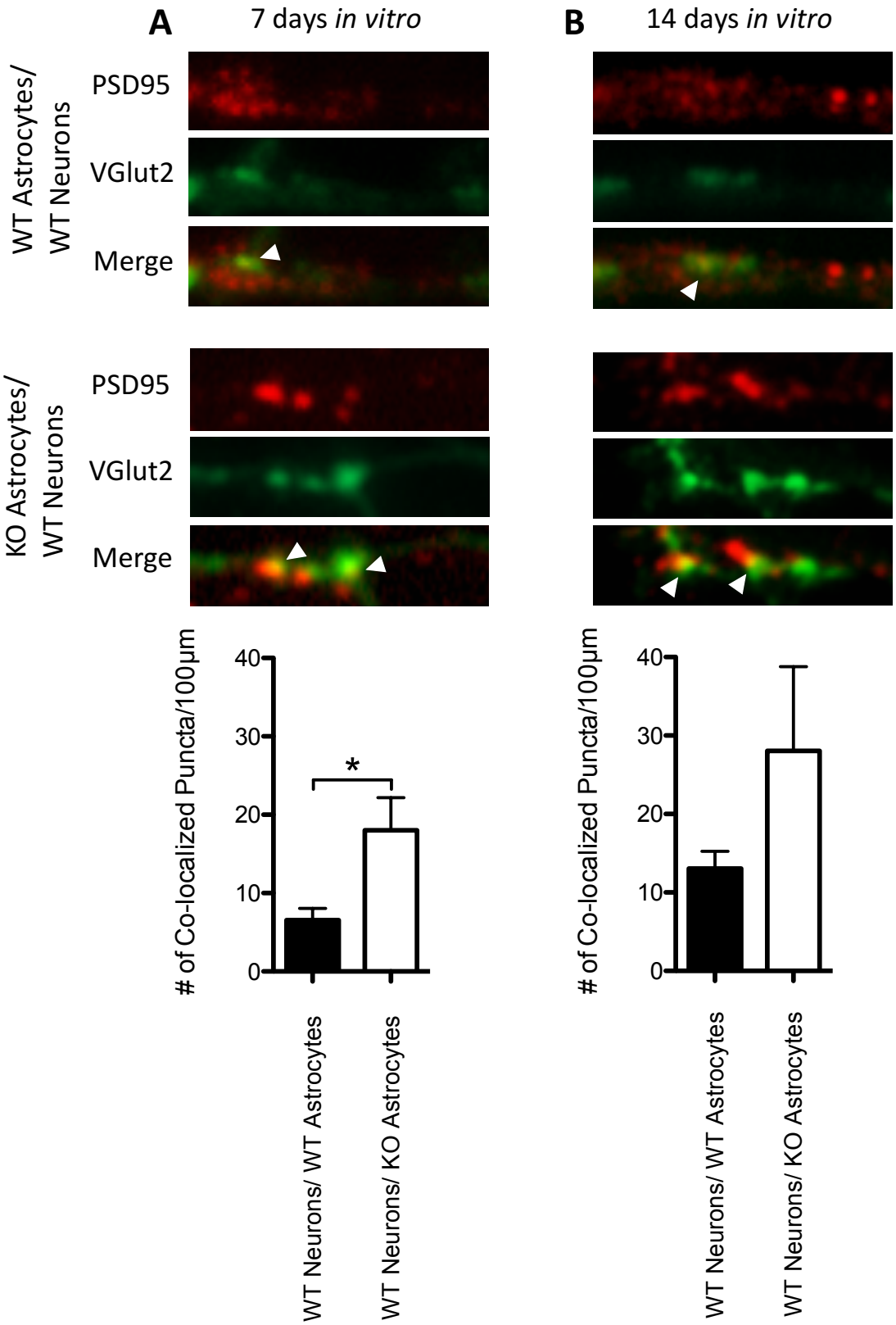
A
7 days *in vitro*
B
14 days *in vitro*
WT Astrocytes/ WT Neurons
PSD95
VGlut2
Merge
KO Astrocytes/ WT Neurons
PSD95
VGlut2
Merge
# of Co-localized Puncta/100µm
40
30
20
10
0
*
WT Neurons/ WT Astrocytes
WT Neurons/ KO Astrocytes
# of Co-localized Puncta/100µm
40
30
20
10
0
WT Neurons/ WT Astrocytes
WT Neurons/ KO Astrocytes

Figure 13. At 7 *DIV* the number of VGlut2$^+$/ PSD95$^+$ co-localized puncta is increased in co-cultures of *Fmr1* KO astrocytes (isolated from P1 pups) and WT neurons, relative to co-cultures of WT astrocytes and WT neurons. WT cortical and thalamic neurons were isolated from P1 pups via MACS separation and co-cultured with either WT or *Fmr1* KO astrocytes isolated from P1 pups. Co-cultures were maintained for either **(A)** 7 days *in vitro* or **(B)** 14 days *in vitro* and subsequently co-labelled with antibodies against vesicular glutamate transporter-2 (VGlut2) and post-synaptic density protein 95 (PSD95) to visualize pre-synaptic and post-synaptic puncta, respectively. White arrows indicate co-localized Vglut2$^+$ (green) and PSD95$^+$ (red) puncta. Measures of thalamocortical synapse number (identified by the co-localized VGlut2$^+$ and PSD95$^+$ puncta) were obtained from cultures containing WT astrocytes (black; N=1, n=10) and cultures containing *Fmr1* KO astrocytes (white; N=1, n=10) and normalized to dendrite length. Images were obtained using a 40x objective with a Zeiss Axioimager. M2. (*$P <$ 0.05)

CHAPTER FIVE

DISCUSSION AND CONCLUSION

5.1 Hevin, SPARC, and GPC 4/6 levels in the cortex and hippocampus of *Fmr1* KO mice, relative to WT mice

The first few weeks of postnatal development are a time of vigorous growth, maturation, and pruning or elimination of synapses. These events must occur in a highly concerted fashion in order to establish proper synaptic connections and neuronal circuitry. Alterations in the development of synaptic structures are a hallmark of FXS (Comery et al., 1997; Irwin et al., 2000; Irwin et al., 2001; Nimchinsky et al., 2001). Astrocytes play a significant role in the regulation of synaptic development and astrocyte dysfunction has recently been linked to neurodevelopmental disorders such as FXS (reviewed in Sloan and Barres, 2014). Our findings suggest that aberrant astrocyte-signalling occurs in the absence of FMRP. In this study, we examined the expression of the astrocyte-secreted factors hevin, SPARC, and GPC 4/6, which have been implicated in the regulation of proper excitatory synapse development and maturation. This study is the first to investigate these factors within the context of FXS. Interestingly, we found altered protein levels of two factors, hevin and SPARC, in *Fmr1* KO mice compared to WT controls; however, protein expression patterns varied between the two brain regions examined, the cortex and the hippocampus. Specifically, in the cortex of *Fmr1* KO mice, we found a transient increase in hevin levels at P14, as well as a decrease in SPARC at P7 and P14, compared to WT controls. Surprisingly, in the hippocampus of *Fmr1* KO mice hevin expression was much lower than that of the WT group at P7. The levels of hevin in the *Fmr1* KO group increased to levels similar to the WT group by P14, and surpassed WT levels by P21.

The most profound differences between genotypes that we observed were in hevin expression levels in both the cortex and hippocampus. Hevin is highly expressed in astrocytes during development, as well as during adulthood (Cahoy et al., 2008; Mendis et al., 1996).

Microarray studies have shown an upregulation of *Hevin* transcripts present in the cerebellum of ASD patients (Purcell et al., 2001). Whole-genome sequencing has additionally identified possible ASD-associated mutations in *Hevin* (De Rubeis et al., 2014), which may alter the expression or function of hevin in these individuals. Here, we show that alterations in the expression of hevin also occurred in a mouse model of FXS. Perhaps this is not surprising given that hevin is a known target of FMRP (Darnell et al., 2011), but the differential expression across the brain regions and developmental time points suggest that its role is not only spatially complex but also highly dependent on temporal regulation.

We observed a transient increase in hevin in the cortex of P14 *Fmr1* KO mice, a time during which intracortical and thalamocortical connections are actively being established and are not yet mature (Nakamura et al., 2005). In the cortex, excitatory synapses are primarily formed via thalamic and intracortical axonal projections that contact dendritic spines. Several lines of evidence suggest that hevin is required for the proper establishment and maintenance of thalamocortical connections. Risher et al. (2014) reported a profound reduction in thalamocortical synapses in Layer 1 of the primary visual cortex of *Hevin* KO mice at postnatal day 7, day 25, and week 12. Interestingly, this was accompanied by a transient increase in intracortical synapses at P25, a possible compensation for the reduced number of thalamocortical connections. These findings *in vivo* were supported by findings from cultured neurons. When cortical and thalamic neurons collected from *Hevin* KO mice were grown together in the presence of hevin-containing growth media there was an increase in the number of thalamocortical synapses, compared to cultures grown in media that did not contain hevin.

Moreover, a subsequent study found that hevin works to establish thalamocortical connections by bridging neurexin-1α and neuroligin-1B (Singh et al., 2016), two trans-synaptic

molecules abundantly expressed in the brain (Schreiner et al., 2016). While neurexins are found to link with vesicle-release apparatus from the pre-synaptic cell, neuroligins are linked with various postsynaptic receptors (Chubykin et al., 2007; Craig and Kang, 2007; Lee et al., 2010; Budreck et al., 2013). As such, trans-synaptic neurexin and neuroligin pairs are able to align pre-synaptic components with post-synaptic components (Scheffele et al., 2000; Graf et al., 2004). Thus, the adhesion between presynaptic neurexin and postsynaptic neuroligin pairs is crucial for the establishment and proper maturation of synapses (Südhof, 2008; Baudouin and Scheiffele, 2010). While particular neurexin and neuroligin pairs interact strongly with one another, neurexin-1α has a very weak affinity for neuroligin-1B (Boucard et al., 2005; Chih et al., 2006) and thus this pair requires hevin to act as a linker molecule. Taken together, these studies indicate that hevin directly influences the number of thalamocortical synapses, and by doing so may indirectly effect the number of intracortical synapses.

Similar to the under expression of hevin, an excess of hevin during critical developmental windows could also contribute to alterations in thalamocortical and intracortical connectivity. This possibility is consistent with findings of altered cortical function and connectivity in FXS. In the barrel cortex of two-week-old *Fmr1* KO mice several defects in Layer III to IV synaptic connectivity have been reported, including reduced strength, diffuse axonal arbors, and altered experience-dependent plasticity (Bureau et al., 2008). These defects were transient and were not observed in 3-week-old mice. Likewise, Cruz-Martin et al. (2010) described a higher turnover-rate of dendritic spines of Layer II/III pyramidal neurons during the second postnatal week of *Fmr1* KO mice, indicating a delay in the stabilization of these spines. The critical period for thalamocortical plasticity in the barrel cortex of mice (somatosensory layer IV), which normally occurs during the first postnatal week, is delayed in *Fmr1* KO mice, potentially a reflection of

the increase in the number of 'silent' synapses at earlier time points (Harlow et al., 2010). Wang et al. (2014) observed an increase in the number of thalamocortical synapses in layer IV of the somatosensory cortex of *Fmr1* KO mice, compared to WT mice. Additionally, abnormal thalamocortical connectivity has been indicated in ASD (Cheon et al., 2011; Mizuno et al., 2006; Nair et al., 2013). The increase in cortical hevin levels in P14 *Fmr1* KO mice found here may contribute to developmental delays in the maturation and stabilization of synapses in the cortex. Interestingly, the majority of the above phenotypes within the FXS cortex are transient and appear to normalize by adulthood, consistent with the return of *Fmr1* KO hevin levels to WT levels by P21. Additionally, it would be interesting to determine whether there are alterations in the expression levels of neurexin-1α and neuroligin-1B, concomitant with the increase that we observed in hevin expression in the cortex of P14 *Fmr1* KO mice. Interestingly, Lai et al. (2016) reported sex-specific genotypic differences in the mRNA expression of various neurexin and neuroligin transcripts. In particular, Lai et al. found a decrease in neurexin-1 mRNA in the somatosensory cortex of P7 *Fmr1* KO females, compared to age-and-sex-matched WT mice. More work must be done to determine the expression patterns of particular isoforms and splice variants of neurexins and neuroligins, respectively. Perhaps altered expression of neurexin-1α and neuroligin-1B also contributes to the government of thalamocortical synapse formation.

Although we also found genotypic differences in hevin levels in the hippocampus, the pattern of hevin expression that we observed in this region was distinct from that observed in the cortex, suggesting an alternate mechanism by which astrocytes modulate the development of neuronal circuits in distinct brain regions. We found that hevin expression in the hippocampus of P7 *Fmr1* KO mice is much lower than in WT controls, a time-point that directly coincides with maximal FMRP expression in the hippocampus (Lu et al., 2004). While effects to spine and

synapse phenotypes in the hippocampus of *Hevin* KO mice are unknown, there are pronounced deficits in the number of excitatory synapses at P14 and morphological deficits in excitatory synapses at P14 and P25 in the superior colliculus (Kucukdereli et al., 2011). Additionally, in Layer 1 of the primary visual cortex at P25, hevin KO mice show an increase in the number of filopodia-like immature dendritic spines, concomitant with a decrease in mature spines (Risher et al., 2014). Notably, these phenotypes are similar to neurobiological abnormalities found in the hippocampus of *Fmr1* KO mice, which include a reduction in the number of spines that co-localize with synaptic markers (Antar et al., 2006) and delayed synapse maturation (Braun and Segal, 2000). A reduced level of hevin in the hippocampus, such as we observed here, may contribute to the defects in dendritic spines and synapses found in the hippocampus of *Fmr1* KO mice.

Although very low at P7, protein expression of hevin in the hippocampus of *Fmr1* KO mice increased to WT levels by P14, and then exceeded WT levels by P21. This discrepancy may be indicative of a shift in the role of hevin from promoting synapse formation during early postnatal development to modulating synaptic function and plasticity during adulthood. In agreement with this, hevin has been shown to exhibit anti-adhesive properties (Gongidi et al., 2004). The presence of hevin may enhance synaptic plasticity by reducing cell adhesion and promoting spine remodelling. Additionally, hevin contains a highly conserved calcium binding domain (Hambrock et al., 2003) and may modulate synaptic function by regulating local calcium concentrations. Indeed, more studies are needed to further elucidate the role of hevin in the brain during development and adulthood, and particularly in regard to FXS. It would also be interesting to see if hevin levels remain elevated at later time-points in adulthood in *Fmr1* KO mice.

In addition to hevin, we examined protein levels of SPARC. SPARC is highly expressed by astrocytes in the developing brain and is capable of inhibiting the synaptogenic function of hevin (Cahoy et al., 2008; Kucukdereli et al., 2011). Due to the antagonism between SPARC and hevin, we postulated that the expression of SPARC may also differ in *Fmr1* KO mice as part of a homeostatic mechanism to compensate for alterations in hevin. However, we found only modest decreases in SPARC in the cortex of *Fmr1* KO mice at P7 and P14; and SPARC expression did not differ between genotypes at P21 in the cortex or at any time-points examined for the hippocampus. Taken together, these findings indicate that SPARC does not compensate for alterations in hevin expression. In fact, the decrease in SPARC at P14 in the cortex coincides with a robust increase in hevin, thus providing a permissive environment for the synaptogenic activity of hevin.

Excitatory synapses within the central nervous system are predominantly glutamatergic. As these synapses begin to establish, they express only NMDA receptors at the post-synaptic membrane and are 'silent', meaning that they lack post-synaptic function. This is followed by the recruitment of AMPA receptors to the postsynaptic membrane, thus inciting postsynaptic function (Isaac et al., 1999). While hevin induces the formation of silent synapses, SPARC and GPC 4/6 have been identified as negative and positive regulators of AMPA receptors at the postsynaptic membrane, respectively (Jones et al., 2011; Allen et al., 2012). We found a modest, but significant, decrease in SPARC at P7 and P14 and a trend towards a decrease in GPC 4/6 in the cortex of P21 *Fmr1* KO mice. Although the decrease in GPC 4/6 was not significant, this may point to significant differences at other time-points that we were unable to detect with our methods. Given this, altered levels of these factors in FXS may also contribute to a dysregulation of AMPA receptors. To what extent the expression of AMPA receptors may be

altered in FXS in a brain-region-specific manner is still under debate (reviewed in Uzunova et al., 2014), and so the further assessment of the regulation of AMPA receptors in various brain regions at various developmental time-points in FXS will help to discern its role in FXS.

5.2 VGlut2$^+$/PSD95$^+$ synapse candidates in co-cultures of astrocytes and neurons

Keeping in mind the role of hevin in the establishment and maintainance of excitatory thalamocortical synapses (Risher et al., 2014; Singh et al., 2016), we sought to determine whether WT cortical and thalamic neurons developed differing numbers of thalamocortical synapses when co-cultured with *Fmr1* KO astrocytes, compared to co-culturing with WT astrocytes. To this end, we co-labelled these astrocyte and neuron co-cultures with antibodies against VGlut2, which is expressed pre-synaptically by the vast majority of thalamocortical synapses (Kaneko and Fujiyama, 2002), and PSD95. Thalamocortical synapses were identified by the co-localization of these pre-synaptic and post-synaptic markers. Interestingly, we found increased numbers of thalamocortical synapses in co-cultures of *Fmr1* KO astrocytes and WT neurons, relative to co-cultures of WT astrocytes and WT neurons, indicating a role for astrocytes in the proper establishment of thalamocortical synapses. It is worth noting, however, that these results derive from one independent culture per group and as such are preliminary. More independent cultures need to be analyzed to corroborate the results presented within this document.

It is well established that FXS is associated with hypersensitivity to sensory stimuli (Marco et al., 2011). Altered thalamocortical connectivity in the absence of FMRP provides a possible mechanism for deficits in the processing of sensory information. Our finding of altered thalamocortical connectivity is consistent with results from Wang et al. (2014) that show an

increase in the number of thalamocortical synapses in layer IV of the somatosensory cortex of 4 month-old *Fmr1* KO mice, compared to WT mice. Importantly, the majority of thalamic inputs project to layer IV of the cortex (Kaneko and Fujiyama, 2002; Khan et al., 2011). Intriguingly, Wang et al. (2014) also reported an increase in the number of thalamocortical connections made onto layer V of the somatosensory cortex in *Fmr1* KO mice, suggesting that molecular mechanisms regulating the establishment of thalamocortical connections vary among sub-regions within the cortex. It would be interesting determine whether different cortical sub-regions exhibit different protein expression patterns of hevin in *Fmr1* KO mice and to determine if alterations in hevin expression correlates with deficits in thalamocortical connectivity across these sub-regions.

It would also be interesting to examine whether the increase that we observed in the number of thalamocortical synapses coincides with an increase in the number of dendritic spines with multiple excitatory contacts (SMECs). Multiply innervated spines, identified by Jones and Powell in 1969, are present during early postnatal development. While the majority of multiply innervated dendritic spines consist of one excitatory input and one inhibitory input, a small fraction of multiply innervated dendritic spines exhibit multiple excitatory connections (Knott et al., 2002; Chen et al., 2012). These SMECs generally disappear by the end of the third postnatal week. Risher et al. (2014) reported an increased number of SMECs in the primary visual cortex of P21 *Hevin* KO mice compared to WT mice. Additionally, Risher et al. demonstrated that the majority of these SMECs received contact from both thalamic and cortical inputs rather than from multiple cortical inputs and suggested that SMECs may act as a site of competition for the establishment of thalamic and cortical inputs. Thus, they concluded that hevin plays a role in the resolution of these SMECs into single-synapse dendritic spines. An excess of hevin, such as we

observed in the cortex of P14 *Fmr1* KO mice, may also disturb the mechanisms underlying synaptic competition between these thalamocortical and corticocortical inputs. Consequently, the increase that we observed in thalamocortical synapses may correspond to an increase in the number of SMECs, reflecting a failure of these SMECs to mature to singly-innervated dendritic spines.

5.3 Conclusion

In this study, we found altered levels of hevin and SPARC in the *Fmr1* KO mouse that suggests aberrant astrocyte-signalling in the absence of FMRP. Expression patterns of these factors differed between time-points and brain regions, demonstrating both spatial and temporal differences in astrocyte regulatory mechanisms. Additionally, we show preliminary data indicating that the number of thalamocortical synapses is increased in co-cultures of *Fmr1* KO astrocytes and WT neurons, relative to co-cultures of WT astrocytes and WT neurons. These findings provide important groundwork for future studies focused on elucidating the roles of both hevin and SPARC throughout development and adulthood to help understand astrocyte-derived regulation of neural circuits. Moreover, these findings emphasize the temporal and regional complexity of this neurodevelopmental disorder. The brain houses a highly heterogeneous array of synapse populations (Emes and Grant, 2012), and the absence of FMRP results in a vast range of abnormal synaptic phenotypes that varies according to brain region and stage of development. This extraordinary level of complexity has led to difficulties in designing effective treatments for FXS as well as other neurodevelopmental disorders. Identifying astrocyte-based molecular mechanisms that are altered in the FXS brain may provide insight into

novel therapeutic strategies more suitable for the treatment of a broad range of neurobiological deficits, as is presented in FXS.

REFERENCES

Allen, N.J., 2013. Role of glia in developmental synapse formation. Curr. Opin. Neurobiol. 23, 1027–1033.

Allen, N.J., Bennett, M.L., Foo, L.C., Wang, G.X., Chakraborty, C., Smith, S.J., Barres, B.A., 2012. Astrocyte glypicans 4 and 6 promote formation of excitatory synapses via GluA1 AMPA receptors. Nature 486, 410–414.

Antar, L.N., Li, C., Zhang, H., Carroll, R.C., Bassell, G.J., 2006. Local functions for FMRP in axon growth cone motility and activity-dependent regulation of filopodia and spine synapses. Mol. Cell. Neurosci. 32, 37–48.

Ashley, C.T., Wilkinson, K.D., Reines, D., and Warren, S.T., 1993. FMR1 protein: conserved RNP family domains and selective RNA binding. Science 262, 563–566.

Bakker, C.E., Verheij, C., Willemsen, R., van der Helm, R., Oerlemans, F., Vermey, M., 1994. Fmr1 knockout mice: A model to study fragile X mental retardation. Cell, 78, 23–33.

Bakker, C.E., de Diego Otero, Y., Bontekoe, C., Raghoe, P., Luteijn, T., Hoogeveen, A.T., Oostra, B.A, Willemsen, R., 2000. Immunocytochemical and biochemical characterization of FMRP, FXR1P, and FXR2P in the mouse. Exp. Cell Res. 258, 162–170.

Baudouin, S., Scheiffele, P., 2010. SnapShot: neuroligin-neurexin complexes. Cell 141, 908.

Beckel-Mitchener, A., Greenough, W.T., 2004. Correlates across the structural, functional, and molecular phenotypes of fragile X syndrome. Dev. Dis. Res. Rev. 10, 53–59.

Berry-Kravis, 2014. Mechanism-based treatments in neurodevelopmental disorders: fragile X syndrome. Pediatr. Neurol 50, 297-302.

Bhakar, A.L., Dölen, G., Bear, M.F., 2012. The pathophysiology of fragile X (and what it

teaches us about synapses). Annu. Rev. Neurosci. 35, 417–443.

Boucard, A.A., Chubykin, A.A., Comoletti, D., Taylor, P., and Südhof, T.C., 2005. A splice code for trans-synaptic cell adhesion mediated by binding of neuroligin 1 to alpha- and beta-neurexins. Neuron 48, 229–236.

Budreck, E.C., Kwon, O.B., Jung, J.H., Baudouin, S., Thommen, A., Kim, H.S., Fukazawa, Y., Harada, H., Tabuchi, K., Shigemoto, R., 2013. Neuroligin-1 controls synaptic abundance of NMDA-type glutamate receptors through extracellular coupling. Proc. Natl. Acad. Sci. USA 110, 725–730.

Bureau, I., Shepherd, G.M.G., Svoboda, K., 2008. Circuit and Plasticity Defects in the Developing Somatosensory Cortex of Fmr1 Knock-Out Mice. J. Neurosci. 28, 5178–5188.

Cahoy, J.D., Emery, B., Kaushal, A., Foo, L.C., Zamanian, J.L., Christopherson, K.S., Xing, Y., Lubischer, J.L., Krieg, P., Krupenko, S.A., Thompson, W.J., Barres, B.A., 2008. A transcriptome database for astrocytes, neurons, and oligodendrocytes: a new resource for understanding brain development and function. J. Neurosci. 28, 264–278.

Chen JL, Villa KL, Cha JW, So PT, Kubota Y, Nedivi E. 2012. Clustered dynamics of inhibitory synapses and dendritic spines in the adult neocortex. Neuron 74:361–373. doi:

Cheon, K.A., Kim, Y.S., Oh, S.H., Park, S.Y., Yoon, H.W., Herrington, J., Nair, A., Koh, Y.J., Jang, D.P., Kim, Y.B., Leventhal, B.L., Cho, Z.H., Castellanos, F.X., Schultz, R.T., 2011. Involvement of the anterior thalamic radiation in boys with high functioning autism spectrum disorders: a diffusion tensor imaging study. Brain Res. 1417, 77–86.

Chih, B., Gollan, L., and Scheiffele, P., 2006. Alternative splicing controls selective trans-synaptic interactions of the neuroligin-neurexin complex. Neuron 51, 171–178.

Chubykin, A.A., Atasoy, D., Etherton, M.R., Brose, N., Kavalali, E.T., Gibson, J.R., and Su¨ dhof, T.C., 2007. Activity-dependent validation of excitatory versus inhibitory synapses by neuroligin-1 versus neuroligin-2. Neuron 54, 919–931.

Chung, W., Allen, N.J., Eroglu, C., 2015. Astrocytes control synapse formation, function, and elimination. Cold Spring Harb. Perspect. Biol. 7, a020370.

Coffee B, Keith K, Albizua I,Malone T, Mowrey J, 2009. Incidence of fragile X syndrome by newborn screening for methylated FMR1 DNA. Am. J. Hum. Genet. 85, 503–14.

Comery, T.A., Harris, J.B., Willems, P.J., Oostra, B.A., Irwin, S.A., Weiler, I.J., Greenough, W.T., 1997. Abnormal dendritic spines in fragile X knockout mice: maturation and pruning deficits. Proc. Natl. Acad. Sci. USA 94, 5401–5404.

Contractor, A., Klyachko, V.A., Portera-Cailliau, C., 2015. Altered Neuronal and Circuit Excitability in Fragile X Syndrome. Neuron 87, 699-715.

Corty, M.M, Freeman, M.R., 2013. Architects in neural circuit design: glia control neuron numbers and connectivity. J. Cell Biol. 203, 395-405.

Craig, A.M., and Kang, Y., 2007. Neurexin-neuroligin signaling in synapse development. Curr. Opin. Neurobiol. 17, 43–52.

Cruz-Martin, A., Crespo, M., Portera-Cailliau, C., 2010. Delayed stabilization of dendritic spines in fragile X mice. J. Neurosci. 30, 7793–7803.

Darnell, J.C., Van Driesche, S.J., Zhang, C., Hung, K.Y.S., Mele, A., Fraser, C.E., Stone, E.F., Chen, C., Fak, J.J., Chi, S.W., Licatalosi, D.D., Richter, J.D., Darnell, R.B., 2011. FMRP stalls ribosomal translocation on mRNAs linked to synaptic function and autism. Cell 146, 247–261.

De Cat, B., David, G., 2001. Developmental roles of the glypicans. Semin. Cell Dev. Biol. 12, 117–125.

De Rubeis, S., He, X., Goldberg, A.P., Poultney, C.S., Samocha, K., Cicek, E.A., Kou, Y., Liu, L., Fromer, M., Walker, S., Singh, T., Klei, L., Kosmicki, J., Fu, S.C., Aleksic, B., Biscaldi, M., Bolton, P.F., Brownfeld, J.M., Cai, J., Campbell, N.J., Carracedo, A., Chahrour, M.H., Chiocchetti, A.G., Coon, H., Crawford, E.L., Crooks, L., Curran, S.R., Dawson, G., Duketis, E., Fernadez, B.A., Gallagher, L., Geller, E., Guter, S.J., Hill, S.R., Lonita-Laza, L., Gonzalez, P.J., Kilpinen, H., Klauck, S.M., Kolevzon, A., Lee, I., Lei, J., Lehtimaki, T., Lin, C.F., Ma'ayan, A., Marshall, C.R., McInnes, A.L., Neale, B., Owen, M.J., Ozaki, N., Parellada, M., Parr, J.R., Purcell, S., Puura, K., Rajagopalan, D., Rehnstrom, K., Reichenberg, A., Sabo, A., Sachse, M., Sanders, S.J., Schafer, C., Schulte-Ruther, M., Skuse, D., Stevens, C., Szatmari, P., Tammimies, K., Valladares, O., Voran, A., Wang, L.-S., Weiss, L.A., Willsey, A.J., Yu, T.W., Yuen, R.K., The DDD Study, Homozygosity Mapping Collaborative for Autism, UK10K Consortium, the Autism Sequencing Consortium, Cook, E.H., Freitag, C.M., Gill, M., Hultman, C.M., Lehner, T., Palotie, A., Schellenberg, G.D., Sklar, P., State, M.W., Sutcliffe, J.S., Walsh, C.A., Scherer, S.W., Zwick, M.E., Barrett, J.C., Cutler, D.J., Roeder, K., Devlin, B., Daly, M.J., Buxbaum, J.D., 2014. Synaptic, transcriptional, and chromatin genes disrupted in autism. Nature 515, 209–215.

Emes, R.D., Grant, S.G.N., 2012. Evolution of synapse complexity and diversity. Annu. Rev. Neurosci 35, 111–131.

Feng Y, Gutekunst CA, Eberhart DE, Yi H, Warren ST, Hersch SM. 1997. Fragile X mental retardation protein: nucleocytoplasmic shuttling and association with

somatodendritic ribosomes. J. Neurosci. 17:1539–1547.

Fernandez-Carvajal I, Lopez Posadas B, Pan R, Raske C, Hagerman PJ, Tassone F. 2009. Expansion of an FMR1 grey-zone allele to a full mutation in two generations. J Mol Diagn 11:306–310.

Fremeau, R.T., Jr, Troyer, M.D., Pahner, I., Nygaard, G.O., Tran, C.H., Reimer, R.J., Bellocchio, E.E., Fortin, D., Storm-Mathisen, J., Edwards, R.H., 2001 The expression of vesicular glutamate transporters defines two classes of excitatory synapse. Neuron 31, 247–260.

Fu YH, Kuhl DP, Pizzuti A, Pieretti M, Sutcliffe JS, Richards S, Verkerk AJ, Holden JJ, Fenwick RG, Warren ST. 1991. Variation of the CGG repeat at the fragile X site results in genetic instability: resolution of the Sherman paradox. Cell 67:1047–1058.

Garber, K.B., Visootsak, J., and Warren, S.T., 2008. Fragile X syndrome. Eur. J. Hum. Genet. 16, 666–672.

Graf, E.R., Zhang, X., Jin, S.X., Linhoff, M.W., and Craig, A.M., 2004. Neurexins induce differentiation of GABA and glutamate postsynaptic specializations via neuroligins. Cell 119, 1013–1026.

Graziano, A., Liu, X-B., Murray, K.D., Jones, E.G., 2008. Vesicular glutamate transporters define two sets of glutamatergic afferents to the somatosensory thalamus and two thalamocortical projections in the mouse. J. Comp. Neurol 507, 1258–1276.

Gongidi, V., Ring, C., Moody, M., Brekken, R., Sage, E.H., Rakic, P., Anton, E.S., 2004. SPARC-like 1 regulates the terminal phase of radial glia-guided migration in the cerebral cortex. Neuron 41, 57–69.

Hambrock, H.O., Nitsche, D.P., Hansen, U., Bruckner, P., Paulsson, M., Maurer, P., Hartmann, U., 2003. SC1/hevin: An extracellular calcium-modulated protein that binds collagen I.J.

Biol. Chem. 278, 11351–11358.

Harlow, E.G., Till, S.M., Russell, T.A., Wijetunge, L.S., Kind, P., Contractor, A., 2010. Critical period plasticity is disrupted in the barrel cortex of Fmr1 knockout mice. Neuron 65, 385–398.

Harrison, C.J., Jack, E.M., Allen, T.D., Harris, R., 1983. The fragile X: a scanning electron microscope study. J. Med. Genet. 20, 280–285.

Hou, L., Antion, M.D., Hu, D., Spencer, C.M., Paylor, R., Klann, E., 2006. Dynamic translational and proteasomal regulation of fragile X mental retardation protein controls mGluR-dependent long-term depression. Neuron 51, 441–454.

Ivanov, A., Esclapez, M., Ferhat, L., 2009. Role of drebrin A in dendritic spine plasticity and synaptic function: Implications in neurological disorders. Commun Integr Biol. 2, 268-70.

Irwin, S.A., Galvez, R., Greenough, W.T., 2000. Dendritic spine structural anomalies in fragile-X mental retardation syndrome. Cereb. Cortex 10, 1038–1044.

Irwin, S.A., Patel, B., Idupulapati, M., Harris, J.B., Crisostomo, R.A., Larsen, B.P., Kooy, F., Willems, P.J., Cras, P., Kozlowski, P.B., Swain, R.A., Weiler, I.J., Greenough, W.T., 2001. Abnormal dendritic spine characteristics in the temporal and visual cortices of patients with fragile-X syndrome: a quantitative examination. Am. J. Med. Genet. 98, 161–167.

Isaac, J.T.R., Nicoll, R.A., Malenka, R.S., 1999. Silent glutamatergic synapses in the mammalian brain. Can. J. Physiol. Pharmacol. 77, 735–737.

Jacobs, S., Doering, L.C., 2009. Primary dissociated astrocyte and neuronal co-culture, in: Doering, L.C., (ed) Protocols for Neural Cell Culture, Ed 4, Humana, New York, pp. 269–248.

Jones, E.G., Powell, T.P., 1969. Morphological variations in the dendritic spines of the

neocortex. Journal of Cell Science 5, 509–529.

Jones, E.V., Bernardinelli, Y., Tse, Y.C., Chierzi, S., Wong, T.P., Murai, K.K., 2011. Astrocytes control glutamate receptor levels at developing synapses through SPARC-beta-integrin interactions. J. Neurosci. 31, 4154–4165.

Kaneko, T., Fujiyama, F., 2002. Complementary distribution of vesicular glutamate transporters in the central nervous system. Neuroscience Research 42, 243–250.

Khan, Z.U., Martín-Montañez, E., Baxter, M.G., 2011. Visual perception and memory systems: from cortex to medial temporal lobe. Cellular and Molecular Life Sciences 68, 1737–1754.

Knott, G.W., Quairiaux, C., Genoud, C., Welker, E., 2002. Formation of dendritic spines with GABAergic synapses induced by whisker stimulation in adult mice. Neuron 34, 265–273.

Kronk, R., Bishop, E.E., Raspa, M., Bickel, J.O., Mandel, D.A., Bailey, D.B. Jr., 2010. Prevalence, nature, and correlates of sleep problems among children with fragile X syndrome based on a large scale parent survey. Sleep 33, 679-687.

Kucukdereli, H., Allen, N.J., Lee, A.T., Feng, A., Ozlu, M.I., Conatser, L.M., Chakraborty, C., Workman, G., Weaver, M., Sage, E.H., Barres, B.A., Eroglu, C., 2011. Control of excitatory CNS synaptogenesis by astrocyte-secreted proteins Hevin and SPARC. PNAS 108, E440–E449.

Lai, J.K.Y., Doering, L.C., Foster, J.A., 2016. Developmental expression of the neuroligins and neurexins in fragile x mice. J. Comp. Neurol., 524, 807-828.

Lee, H., Dean, C., and Isacoff, E., 2010. Alternative splicing of neuroligin regulates the rate of presynaptic differentiation. J. Neurosci. 30, 11435–11446.

Lu, R., Wang, H., Liang, Z., Ku, L., O'Donnell, W.T., Li, W., Warren, S.T., Feng, Y., 2004. The fragile X protein controls microtubule-associated protein 1B translation and microtubule

stability in brain neuron development. Proc. Natl. Acad. Sci. USA 101, 15201–15206.

Lubs, H.A., 1969. A marker X chromosome. American Journal of Human Genetics 21, 231.

Lubs, H.A., Stevenson, R.E., Schwartz, C.E., 2012. Fragile X and X-linked intellectual disability: four decades of discovery. Am. J. Hum. Genet. 90, 579–590.

Marco, E.J., Hinkley, L.B., Hill, S.S., Nagarajan, S.S., 2011. Sensory processing in autism: a review of neurophysiologic findings. Pediatr. Res. 69, 48R–54R.

Martin, J.P., Bell, J., 1943. A pedigree of mental defect showing sex-linkage. J Neurol Psychiatry 6, 154–157.

Mauch, D.H., Nagler, K., Schumacher, S., 2001. CNS synap- togenesis promoted by glia derived cholesterol. Science 294, 1354–1357.

Mendis, D.B., Shahin, S., Gurd, J.W., Brown, I.R., 1996. SC1, a SPARC-related glycoprotein, exhibits features of an ECM component in the developing and adult brain. Brain Res. 713, 53–63.

Mizuno, A., Villalobos, M.E., Davies, M.M., Dahl, B.C., Müller, R.A., 2006. Partially enhanced thalamocortical functional connectivity in autism. Brain Res. 1104, 160–174.

Nair, A., Treiber, J.M., Shukla, D.K., Shih, P., Müller, R.A., 2013. Impaired thalamocortical connectivity in autism spectrum disorder: a study of functional and anatomical connectivity. Brain 136, 1942–1955.

Nakamura, K., Hioki, H., Fujiyama, F., Kaneko, T., 2005. Postnatal changes of vesicular glutamate transporter (VGluT)1 and VGluT2 immunoreactivities and their colocalization in the mouse forebrain. J. Comp. Neurol. 492, 263–288.

Nimchinsky, E.A., Oberlander, A.M., Svoboda, K., 2001. Abnormal development of dendritic spines in FMR1 knock-out mice. J. Neurosci. 21, 5139–5146.

Oberlé, I., Rousseau, F., Heitz, D., Kretz, C., Devys, D., Hanauer, A., Boué, J., Bertheas, M.F., Mandel, J.L., 1991. Instability of a 550-base pair DNA segment and abnormal methylation in fragile X syndrome. Science 252, 1097–1102.

Oostra, B.A., Hoogeveen, A.T., 1997. Animal model for fragile X syndrome. Ann. Med. 29, 563–567.

Pacey, L.K.K., Doering, L.C., 2007. Developmental Expression of FMRP in the Astrocyte Lineage : Implications for Fragile X Syndrome. Glia 55, 1601–1609.

Pfeiffer, B.E., Huber, K.M., 2009. The state of synapses in Fragile X Syndrome. Neuroscientist 15, 549–567.

Pieretti, M., Zhang, F.P., Fu, Y.H., Warren, S.T., Oostra, B.A., Caskey, C.T., Nelson, D.L. 1991. Absence of expression of the FMR-1 gene in fragile X syndrome. Cell 66, 817–822.

Purcell, A.E., Jeon, O.H., Zimmerman, A.W., Blue, M.E., Pevsner, J., 2001. Postmortem brain abnormalities of the glutamate neurotransmitter system in autism. Neurology 57, 1618–1628.

Richards, B.W., Sylvester P.E., Brooker C., 1981. Fragile X-linked mental retardation: the Martin-Bell syndrome. J. Ment. Defic. Res. 25, 253-256.

Risher, W.C., Patel, S., Kim, I.H., Uezu, A., Bhagat, S., Wilton, D.K., Pilaz, L., Singh Alvarado, J., Calhan, O.Y., Silver, D.L., Stevens, B., Calakos, N., Soderling, S.H., Eroglu, C., 2014. Astrocytes refine cortical connectivity at dendritic spines. Elife 3, e04047.

Santoro, M. R., Bray, S. M., and Warren, S. T., 2012. Molecular mechanisms of fragile X syndrome: a twenty-year perspective. Annu. Rev. Pathol. 7, 219–245.

Scheiffele, P., Fan, J., Choih, J., Fetter, R., and Serafini, T., 2000. Neuroligin expressed in nonneuronal cells triggers presynaptic development in contacting

axons. Cell 101, 657–669.

Schreiner, D., Simicevic, J., Ahrne´, E., Schmidt, A., and Scheiffele, P., 2015. Quantitative isoform-profiling of highly diversified recognition molecules. eLife 4, e07794.

Sidorov, M.S., Auerbach, B.D., and Bear, M.F., 2013. Fragile X mental retardation protein and synaptic plasticity. Mol. Brain 6, 15.

Singh, S.K., Stogsdill, J.A., Pulimood, N.S., Dingsdale, H., Kim, Y.H., Pilaz, L.J., Kim, I.H., Manhaes, A.C., Rodrigues, W.S., Pamukcu, A., Enustun, E., Ertuz, Z., Scheiffele, P., Soderling, S.H., Silver, D.L., Ji, R.R., Medina, A.E., Eroglu, C., 2016. Astrocytes assemble thalamocortical synapses by bridging NRX1α and NL1 via hevin. Cell 164, 183–196.

Sloan, S.A., Barres, B.A., 2014. Mechanisms of astrocyte development and their contributions to neurodevelopmental disorders. Curr. Opin. Neurobiol. 27, 75–81.

Südhof, T.C., 2008. Neuroligins and neurexins link synaptic function to cognitive disease. Nature 455, 903–911.

Uzunova, G., Hollander, E., Shepherd, J., 2014. The role of ionotropic glutamate receptors in childhood neurodevelopmental disorders: autism spectrum disorders and Fragile X Syndrome. Curr. Neuropharmacol. 12, 71–98.

Verkerk, A.J.M.H, Pieretti, M., Sutcliffe, J.S., Fu, Y-H, Kuhl, D. P. A., Pizzuti, A., Reiner, O., 1991. Identification of a gene (FMR-1) containing a CGG repeat coincident with a breakpoint cluster region exhibiting length variation in fragile X syndrome. Cell 65, 905-914.

Wang, G.X., Smith, S.J., Mourrain, P., 2014. *Fmr1* KO and fenobam treatment differentially impact distinct synapse populations of mouse neocortex. Neuron 84, 1273-1286.

Wang, H., Ku, L., Osterhout, D.J., Li, W., Ahmadian, A., Liang, Z., 2004. Developmentally-programmed FMRP expression in oligodendrocytes: a potential role of FMRP in regulating translation in oligodendroglia progenitors. Hum. Mol. Genet. 13, 79-89.

Wang, H., Pati, S., Pozzo-Miller, L., Doering, L.C., 2015. Targeted pharmacological treatment of autism spectrum disorders: fragile X and Rett syndromes. Front. Cell Neurosci. 9, 55.

Wang, T., Bray, S.M., and Warren, S.T., 2012. New perspectives on the biology of fragile X syndrome. Curr. Opin. Genet. Dev. 22, 256–263.

Yrigollen, C.M., Martorell, L., Durbin-Johnson, B., Naudo, M., Genoves, J., Murgia, A., Polli, R., Zhou, L., Barbouth, D., Rupchock, A., 2014. AGG interruptions and maternal age affect FMR1 CGG repeat allele stability during transmission. J. Neurodev. Disord. 6, 24.